



Calhoun: The NPS Institutional Archive
DSpace Repository

NPS Scholarship

Theses

2006-09

Remote sensing of the refractive environment
above the marine stratocumulus-topped
boundary layer

Derley, Dennis T.

Monterey, CA; Naval Postgraduate School

<https://hdl.handle.net/10945/2550>

Downloaded from NPS Archive: Calhoun



Calhoun is the Naval Postgraduate School's public access digital repository for research materials and institutional publications created by the NPS community. Calhoun is named for Professor of Mathematics Guy K. Calhoun, NPS's first appointed -- and published -- scholarly author.

Dudley Knox Library / Naval Postgraduate School
411 Dyer Road / 1 University Circle
Monterey, California USA 93943

<http://www.nps.edu/library>



**NAVAL
POSTGRADUATE
SCHOOL**

MONTEREY, CALIFORNIA

THESIS

**REMOTE SENSING OF THE REFRACTIVE
ENVIRONMENT ABOVE THE MARINE
STRATOCUMULUS-TOPPED BOUNDARY LAYER**

by

Dennis Todd Derley

September 2006

Thesis Advisor:
Second Reader:

Philip A. Durkee
Mary S. Jordan

Approved for public release; distribution is unlimited

THIS PAGE INTENTIONALLY LEFT BLANK

REPORT DOCUMENTATION PAGE			<i>Form Approved OMB No. 0704-0188</i>
Public reporting burden for this collection of information is estimated to average 1 hour per response, including the time for reviewing instruction, searching existing data sources, gathering and maintaining the data needed, and completing and reviewing the collection of information. Send comments regarding this burden estimate or any other aspect of this collection of information, including suggestions for reducing this burden, to Washington headquarters Services, Directorate for Information Operations and Reports, 1215 Jefferson Davis Highway, Suite 1204, Arlington, VA 22202-4302, and to the Office of Management and Budget, Paperwork Reduction Project (0704-0188) Washington DC 20503.			
1. AGENCY USE ONLY (Leave blank)	2. REPORT DATE September 2006	3. REPORT TYPE AND DATES COVERED Master's Thesis	
4. TITLE AND SUBTITLE :Remote Sensing of the Refractive Environment Above the Marine Stratocumulus-Topped Boundary Layer		5. FUNDING NUMBERS	
6. AUTHOR(S) Dennis Todd Derley		8. PERFORMING ORGANIZATION REPORT NUMBER	
7. PERFORMING ORGANIZATION NAME(S) AND ADDRESS(ES) Naval Postgraduate School Monterey, CA 93943-5000		10. SPONSORING/MONITORING AGENCY REPORT NUMBER	
9. SPONSORING /MONITORING AGENCY NAME(S) AND ADDRESS(ES) N/A		11. SUPPLEMENTARY NOTES The views expressed in this thesis are those of the author and do not reflect the official policy or position of the Department of Defense or the U.S. Government.	
12a. DISTRIBUTION / AVAILABILITY STATEMENT Approved for public release; distribution is unlimited.		12b. DISTRIBUTION CODE	
13. ABSTRACT (maximum 200 words) Electro-Magnetic propagation paths are subject to refraction as they travel through moisture and temperature gradients found within the inversion layer at the top of the stratocumulus-topped marine boundary layers (STBL). The NPS Meteorology Department is developing an automated program called SEMEO (Satellite Electro-Magnetic Electro-Optical) that will use remote sensors to estimate the cloud-top height, and characterize the ducting conditions over large regions. In addition to estimating the location and strength of elevated ducts, the probability that each duct will reach the surface will also be assigned by the SEMEO program. This thesis tests the SEMEO program with a unique dataset and provides recommendations as appropriate. Results indicate that the SEMEO cloud-top height algorithm has the most success when the inversion layer is greater than 400m, there is a troughing pattern aloft (500mb level), and there is greater than three degrees Celsius difference between the cloud-top and surface temperature. The SEMEO refractive algorithm over estimates the duct strength by ~100% for shallow boundary layer cases (<400m), and overestimates their corresponding trapping layer depth by ~20%. For deeper boundary layer cases the duct strength was well represented, however, the trapping layer depth was over estimated by ~ 33%.			
14. SUBJECT TERMS Satellite Meteorology, Atmospheric Boundary Layer, Coastal Meteorology, Radar Propagation.		15. NUMBER OF PAGES 85	
		16. PRICE CODE	
17. SECURITY CLASSIFICATION OF REPORT Unclassified	18. SECURITY CLASSIFICATION OF THIS PAGE Unclassified	19. SECURITY CLASSIFICATION OF ABSTRACT Unclassified	20. LIMITATION OF ABSTRACT UL

THIS PAGE INTENTIONALLY LEFT BLANK

Approved for public release; distribution is unlimited

**REMOTE SENSING OF THE REFRACTIVE ENVIRONMENT ABOVE THE
MARINE STRATOCUMULUS-TOPPED BOUNDARY LAYER**

Dennis T. Derley
Lieutenant Commander, United States Navy
B.S., University of LaVerne, 1995

Submitted in partial fulfillment of the
requirements for the degree of

**MASTER OF SCIENCE IN PHYSICAL OCEANOGRAPHY AND
METEOROLOGY**

from the

**NAVAL POSTGRADUATE SCHOOL
September 2006**

Author: Dennis T. Derley

Approved by: Philip A. Durkee
Thesis Advisor

Mary S. Jordan
Second Reader

Philip A. Durkee
Chairman, Department of Meteorology

THIS PAGE INTENTIONALLY LEFT BLANK

ABSTRACT

Electro-Magnetic propagation paths are subject to refraction as they travel through moisture and temperature gradients found within the inversion layer at the top of the stratocumulus-topped marine boundary layers (STBL). The NPS Meteorology Department is developing an automated program called SEMEO (Satellite Electro-Magnetic Electro-Optical) that will use remote sensors to estimate the cloud-top height, and characterize the ducting conditions over large regions. In addition to estimating the location and strength of elevated ducts, the probability that each duct will reach the surface will also be assigned by the SEMEO program. This thesis tests the SEMEO program with a unique dataset and provides recommendations as appropriate. Results indicate that the SEMEO cloud-top height algorithm has the most success when the inversion layer is greater than 400m, there is a troughing pattern aloft (500mb level), and there is greater than three degrees Celsius difference between the cloud-top and surface temperature. The SEMEO refractive algorithm over estimates the duct strength by ~100% for shallow boundary layer cases (<400m), and overestimates their corresponding trapping layer depth by ~20%. For deeper boundary layer cases the duct strength was well represented, however, the trapping layer depth was over estimated by ~ 33%.

THIS PAGE INTENTIONALLY LEFT BLANK

TABLE OF CONTENTS

I.	INTRODUCTION.....	1
A.	MOTIVATION	1
B.	OVERVIEW.....	1
1.	NPS Program.....	1
II.	THEORY	7
A.	ELECTROMAGNETIC PROPAGATION THEORY.....	7
1.	Index of Refraction, Refractivity, Modified Index of Refraction....	7
2.	Definition of Trapping Layers and Ducts.....	10
3.	Formation of Ducts	10
4.	Frequency Dependence on Duct Size	12
B.	CLOUD-TOP TEMPERATURE RETRIEVAL.....	14
C.	ALGORITHM TO ESTIMATE CLOUD-TOP HEIGHT.....	15
D.	ALGORITHM TO ESTIMATE DUCT STRENGTH AND DEPTH.....	17
III.	DATA AND PROCEDURES	23
A.	INSTRUMENTS	23
1.	Moderate Resolution Imaging Spectroradiometer (MODIS)	23
2.	Geostationary Operational Environmental Satellite (GOES)	25
3.	Atmosphere Profile Measurements	25
4.	Sea Surface Temperature (SST) Data.....	26
B.	PROCEDURES	27
1.	Categorizing the Soundings	27
2.	MODIS and GOES Images	32
3.	MODIS and GOES Comparisons.....	33
4.	Cloud-Top Height	35
5.	Modified Index of Refraction (M)	36
6.	MODIS Water Vapor Analysis.....	36
IV.	RESULTS	37
A.	CLOUD TOP HEIGHTS RESULTS	37
1.	Overview	37
2.	Distinguishing Features Between the Cases	40
3.	Case Examples.....	46
B.	MODIFIED INDEX OF REFRACTION (M) RESULTS.....	50
1.	Modifications to Radiosonde Profiles.....	50
2.	Modified Index of Refraction Results for Category 1	52
3.	Modified Index of Refraction Results for Category 2	54
4.	Modified Index of Refraction Results for Category 3	54
5.	Examples of SEMEO's Refractive Results	56
6.	Comparison Between Category 1 and Category 3.....	58
C.	WATER VAPOR ANALYSIS RESULTS.....	59
V.	CONCLUSION AND RECOMMENDATIONS.....	61

A.	CONCLUSIONS	61
B.	RECOMMENDATIONS.....	63
	LIST OF REFERENCES	65
	INITIAL DISTRIBUTION LIST	67

LIST OF FIGURES

Fig. 1.	GOES-10 visual image for 0000 UTC 21 July 2004. Example of the stratocumulus-topped marine boundary layer located off the Vandenberg coast and the approximate relationship between Vandenberg AFB and National Data Buoy Center (NDBC) buoy station 46011.	4
Fig. 2.	World wide frequency of ducting occurrence. From Ortenburger et al (1985).....	5
Fig. 3.	Illustration of sub-refractive, normal, and super-refractive EM propagation categories and the associated gradient values of dN/dz . From Davidson (2005).....	8
Fig. 4.	Modified index of refraction (M) profile vs height (Z), illustrating the trapping layer created when the M gradient is negative. From Davidson (2005).....	9
Fig. 5.	Definition of a trapping layer and its corresponding duct. The red layer indicates where the M gradient is negative, which corresponds with the trapping region. The combined yellow and red layers identify the resulting duct.....	10
Fig. 6.	Three different types of ducts: blue indicates the elevated duct, red is the surface based duct, and green in the evaporative duct. From Davidson (2005).....	11
Fig. 7.	Radar return within an evaporation duct (left) and an elevated surface-based duct (right). From Rogers (1999).....	12
Fig. 8.	Duct thickness required to trap radar frequencies between 0.1 to 100 GHz. From Davidson (2005).....	13
Fig. 9.	Atmospheric transmittance for wavelengths 3.5-13.5 μ m. Transmittance is reduced due to absorption by H ₂ O (blue), CO ₂ (magenta) and ozone (yellow) gases. The spectral width of the GOES (light blue) and MODIS (brown) channels used in this thesis are indicated. From Durkee (2005).....	15
Fig. 10.	Surface temperature (T_s) and satellite infrared cloud-top temperature (T_{CT}) are known values. The lifted condensation level (LCL) is the base of the cloud. The dry adiabatic lapse rate is used in the cloud-free region and the pseudo-adiabatic lapse rate is used in cloud. From Jordan and Durkee (2003).....	17
Fig. 11.	Simulated five-point modified refractive index profile from the SEMEO procedure (red) is compared with the measured radiosonde (blue) from the MAST experiment, 21 June 1994. Points 1-3 are generated from the cloud-top height algorithm. Point 4 is from the trapping layer parameterization technique, and Point 5 is from numerical model estimates of 850mb fields.	18
Fig. 12.	Temperature, $\Delta T'$, which is a parameterization of the temperature increase in the inversion, is computed using the 850mb temperature from each profile, which is warmed dry adiabatically from 850mb to the height of the inversion base. The blue profile on the left represents the dewpoint	

	temperature and the blue profile on the right represents the temperature profile.....	19
Fig. 13.	Example of a Category 1 profile where the magnitude of the gradient for both temperature and dewpoint temperature within the identified trapping layer are similar. Here they both experience a 7.2 °C change. This sounding was launched on 0000 UTC 25 September 2004.....	28
Fig. 14.	Example of a Category 2 profile where the average difference in temperature is at least twice the dewpoint temperature difference within the identified trapping region. Here the temperature difference was 15.4°C and the dewpoint temperature difference was 4.8°C. This sounding was launched on 1200 UTC 11 July 2003.	29
Fig. 15.	Example of a Category 3 profile where the difference in dewpoint temperature is at least twice the temperature difference within the targeted trapping layer. Here the dewpoint temperature difference was 19.9°C and the temperature difference was 0.2°C. This sounding was launched on 1200 UTC 10 June 2003.	30
Fig. 16.	Example of possible erroneous dewpoint temperature values. The cloud top occurs at 521m, yet dewpoint temperature continues to increase for 100 meters. In the 100m layer, relative humidity and M values are assumed to be in error. This sounding was launched at 0000 UTC 31 August 2003.....	32
Fig. 17.	The cloud-top height algorithm typically has success with profiles similar to this Vandenberg sounding at 1200 UTC 16 September 2005. The sounding has a deep cloud layer and a well-defined inversion.....	40
Fig. 18.	500mb heights are superimposed on the GOES-10 infrared image for 1200 UTC 16 September 2005. The 500mb trough over Vandenberg AFB is observed in 11 of 15 cases in Table 8 that have an estimated height error of less than 100m (Image from San Francisco State University 2006).	41
Fig. 19.	Potential temperature and specific humidity graph for 1200 UTC 16 September 2005. The near vertical potential temperature line illustrates the well-mixed boundary layer. The red crosses represent the sounding data points from mandatory and significant reporting levels.....	42
Fig. 20.	Scatterplot of measured cloud-top height (m) versus SEMEO predicted height (m) using SST as the input surface temperature. The black line is the one-to-one line, which indicates no error. The day cases (blue) and night cases (red) are indicated. The RMS error (m) of all 27 cases, 14 day, and 13 night cases is listed.....	43
Fig. 21.	Scatterplot of measured cloud-top height (m) versus SEMEO predicted height (m) using air temperature as the input surface temperature. The black line is the one-to-one line, which indicates no error. The day cases (blue) and night cases (red) are indicated. The RMS error (m) of all 28 cases, 15 day, and 13 night cases is listed.....	44
Fig. 22.	Scatterplot of measured cloud-top height (m) versus SEMEO predicted height (m) using SST as the input surface temperature. The black line is the one-to-one line, which indicates no error. Cases are separated based	

	on brightness temperature and surface temperature difference. Shallow STBL cases (Ch4-SST \geq -3C) are denoted in blue, and deeper STBL cases (Ch4-SST $<$ -3C) are denoted in red. The RMS error (m) of all 27 cases, 10 shallow, and 17 deep cases is listed.....	45
Fig. 23.	Scatterplot of measured cloud-top height (m) versus SEMEO predicted height (m) using air temperature as input. The black line is the one-to-one line, which indicates no error. Cases are separated based on brightness temperature and surface temperature difference. Shallow STBL cases (Ch4-Tair \geq -3C) are denoted in blue, and deeper STBL cases (Ch4-Tair $<$ -3C) are denoted in red. The RMS error (m) of all 28 cases, 14 shallow, and 14 deep cases is listed.	46
Fig. 24.	Vandenberg sounding for 0000 UTC 12 June 2003. The blue lines indicate the temperature and dewpoint temperature profiles. The red line with three red stars superimposed indicates the three points generated from the cloud-top height algorithm (surface, cloud base, and cloud top).....	47
Fig. 25.	500mb height analysis for 0000 UTC 12 June 2003 indicating a trough approaching Vandenberg AFB from the West.....	48
Fig. 26.	Vandenberg AFB sounding for 0000 UTC 28 June 2003. The dewpoint temperature increase above the top of the STBL (266.2m) is assumed to be erroneous.....	49
Fig. 27.	500mb height analysis for 0000 UTC 28 June 2003 indicating a high pressure region above Vandenberg. AFB.	50
Fig. 28.	Modified dewpoint temperature profile for 0000 UTC 5 July 2005. Modifications to the original profile were made to remove dewpoint temperature data points that indicated increased dewpoint values above the cloud top. The blue dashed line represents the original dewpoint temperature profile; the red line is the modified profile.	51
Fig. 29.	Modified RH and M profiles for 0000 UTC 5 July 2005. Modifications to the original profiles were made to remove bad data points that resulted from errors in the dewpoint temperature profile. The blue dashed line represents the original relative humidity and M profiles and the red lines are the modified profiles.	51
Fig. 30.	SEMEO generated profile superimposed on the 0000 UTC 25 September 2004 Vandenberg AFB sounding. The five red stars on the left indicate the SEMEO generated points that are connected to create the predicted M profile. The red stars on the sounding graph on the right indicate the surface, cloud base, clout top, and 850mb height and temperature.	57
Fig. 31.	SEMEO generated profile superimposed on the 1200 UTC 12 June 2003 Vandenberg AFB sounding. The five red stars on the left indicate the SEMEO generated points that are connected to create the predicted M profile. The red stars on the sounding graph on the right indicate the surface, cloud base, clout top, and 850mb height temperature.	58
Fig.32	Scatterplot of predicted M-strength values for Category versus Category 3. The black line is the one-to-one line, which indicates no error	59

THIS PAGE INTENTIONALLY LEFT BLANK

LIST OF TABLES

Table 1.	Numerical values associated with classes of refractivity. From Davidson (2005).....	9
Table 2.	VHF and UHF radar bands and their required duct thickness to be trapped. From Davidson (2005).....	13
Table 3.	MODIS Channel Primary Use and Specifications. (Adapted from GSFC 2003).	24
Table 4.	GOES-10 and GOES 12 Imager	25
Table 5.	Statistics for the first elevated trapping layer (top of STBL) for the 1212 Vandenberg soundings with a negative M gradient. Soundings included are from Apr-Oct 2003-05, and Apr-May 2006.....	31
Table 6.	Nine cases used to determine if a bias exists between MODIS and GOES brightness temperatures.	35
Table 7.	Results from the cloud-top height algorithm, computed using the sea surface temperature, for 30 cases are color-coded by category: Category 1 (black), Category 2 (blue), and Category 3 (green). Input values for the algorithm are the GOES cloud-top brightness temperature (Ch.4, C) and buoy 46011 sea surface temperature (C). Measured cloud-top height (m) is from the Vandenberg AFB radiosonde. Predicted height (m) is the result of the cloud-top height algorithm. Height error (m) is computed and a negative error indicates the algorithm underestimates the height. Predicted height of N/A indicates the input values failed an algorithm requirement and no value was computed.....	38
Table 8.	Results from the cloud-top height algorithm, computed using the air temperature, for 30 cases are color-coded by category: Category 1 (black), Category 2 (blue), and Category 3 (green). Input values for the algorithm are the GOES cloud-top brightness temperature (Ch.4, C) and buoy 46011 air temperature (C). Measured cloud-top height (m) is from the Vandenberg AFB radiosonde. Predicted height (m) is the result of the cloud-top height algorithm. Height error (m) is computed and a negative error indicates the algorithm underestimates the height. Predicted height of N/A indicates the input values failed an algorithm requirement and no value was computed.....	39
Table 9.	Trapping layer statistics for Category 1 cases using SST as the surface temperature input for the SEMEO algorithm. Radiosonde measurements of trapping layer strength (ΔM , unitless) and depth (m) are compared with the SEMEO predictions of strength and depth. Positive errors indicate the SEMEO algorithm overestimated layer strength or depth. The SEMEO algorithm uses a 100m trapping layer depth for all cases.....	53
Table 10.	Trapping layer statistics for Category 1 cases using air temperature as the surface temperature input for the SEMEO algorithm. Radiosonde measurements of trapping layer strength (ΔM , unitless) and depth (m) are compared with the SEMEO predictions of strength and depth. Positive	

	errors indicate the SEMEO algorithm overestimated layer strength or depth. The SEMEO algorithm uses a 100m trapping layer depth for all cases.....	54
Table 11.	Trapping layer statistics for Category 3 cases using SST as the surface temperature input for the SEMEO algorithm. Radiosonde measurements of trapping layer strength (ΔM , unitless) and depth (m) are compared with the SEMEO predictions of strength and depth. Positive errors indicate the SEMEO algorithm overestimated layer strength or depth. The SEMEO algorithm uses a 100m trapping layer depth for all cases.....	55
Table 12.	Trapping layer statistics for Category 3 cases using air temperature as the surface temperature input for the SEMEO algorithm. Radiosonde measurements of trapping layer strength (ΔM , unitless) and depth (m) are compared with the SEMEO predictions of strength and depth. Positive errors indicate the SEMEO algorithm overestimated layer strength or depth. The SEMEO algorithm uses a 100m trapping layer depth for all cases.....	56
Table 13.	MODIS brightness temperatures (C) over Vandenberg AFB for Category 1 and 2 radiosondes. Channels 27-32. are affected by water vapor absorption.....	60
Table 14.	MODIS brightness temperatures (C) over Vandenberg AFB for Category 3 radiosondes. Channels 27-32. are affected by water vapor absorption.....	60

ACKNOWLEDGMENTS

I would like to thank my advisor, Dr. Philip A. Durkee, for his patience and insight throughout the ever changing process. I would like to thank my second reader, Ms. Mary S. Jordan, for her programming expertise and attention to detail. Additionally, thanks to Mr. Bob Creasey, for his availability, experience, and willingness to help throughout my NPS experience. And thanks to Mr. Kurt Neilsen, for his assistance in accessing and retrieving satellite data.

Finally, I would like to thank my family, my wife, Cathy, and son, Reed, for their unwavering support always.

THIS PAGE INTENTIONALLY LEFT BLANK

I. INTRODUCTION

A. MOTIVATION

The Navy Meteorology and Oceanography (METOC) community plays an important role in providing operational support for VHF and microwave electromagnetic (EM) wave propagation. In regions of the atmosphere where changes in temperature, humidity, and pressure exist, ducts can be created. Ducts are regions in the atmosphere where radar signals can be trapped, which may result in extending the radar range well beyond the standard radio horizon, or conversely, create holes in radar coverage. Understanding how the atmosphere can effect EM propagation can then be used to determine the optimum time and location of asset placement in operational areas. This may allow personnel and equipment to get closer than otherwise would have been anticipated, or to attain the objectives while standing off at much further ranges.

B. OVERVIEW

1. NPS Program

EM propagation paths will be altered as they travel through moisture and temperature gradients found within the inversion layer located on top of the stratocumulus-topped marine boundary layers (STBL). The NPS Meteorology Department is developing an automated program called SEMEO (Satellite Electro-Magnetic Electro-Optical) that will use remote sensors to characterize the ducting conditions over large regions. In addition to estimating the location and strength of elevated ducts, a probability of whether each duct will reach the surface will also be assigned by the SEMEO program. This program is funded by the Navy and is designed for stratocumulus-topped marine boundary layers in coastal and open ocean regions. SEMEO is designed to use NPOESS (National Polar-Orbiting Environmental Satellite System) sensors, as well as GOES satellite imagery. The output of SEMEO will be available for input into radar propagation prediction programs to enhance situational awareness within the operational area. The SEMEO program is designed to work in regions where there is a well-defined stratocumulus cloud deck and corresponding inversion just above the cloud top that creates a trapping region.

SEMEO has the following components (Jordan, 2006, personal communication):

1. Marine stratus cloud identification (cloud screen algorithm).
2. Ingest of external temperature field to represent the lower boundary layer at the air-sea interface.
3. Algorithm to estimate cloud-top height.
4. Algorithm to estimate trapping layer strength and depth.
5. Algorithm to estimate the probability of a surface-based duct.
6. Formatting of refractivity information for tactical use.

This thesis will test the SEMEO program using radiosonde data from Vandenberg Air Force Base and sea surface temperature (SST) and air temperature data from the National Data Buoy Center (NDBC) buoy number 46011. These tests will serve as a means to adjust or create new parameterizations within the program.

There are advantages and disadvantages in using the Vandenberg AFB soundings. The advantages include a large accessible dataset at NPS. This thesis analyzes 1297 soundings for the months of April through October 2003-05, and April and May of 2006. This presents the opportunity to test both day and night soundings within the littoral region. This is advantageous because the datasets that were used in the initial SEMEO program include only day time soundings that were located outside the littoral region. The final advantage is the vertical extent of the Vandenberg soundings. Vandenberg soundings provide data from the surface to the top of the troposphere, while the soundings used in setting up the SEMEO program only monitored the lower troposphere. This is important because this study includes analyzing the upper-level water vapor concentrations. There are also disadvantages in using the Vandenberg soundings. One disadvantage is the physical separation from the sounding launch site to the buoy that provides the surface temperature measurement. The distance between the two is approximately 20 miles. This disadvantage was mitigated when determining which cases to test and is described in Chapter 3, section B-4. Another disadvantage is the reporting frequency of the soundings. The Vandenberg soundings report at standard mandatory and significant levels which do not provide as much resolution at the top of the STBL as desired. The final disadvantage was the launching times not being temporally coincident

with the MODIS satellite pass. The MODIS satellite is in a polar orbit and is discussed in Chapter 3, section A-1.

The final portion of this thesis will compare the soundings launched from Vandenberg AFB with water vapor channels available from the satellite-borne remote sensor MODIS (**M**oderate-resolution **I**maging **S**pectroradiometer). The objective in studying the water vapor channels is the role that water vapor plays in refractivity. The goal is to determine if water vapor signatures exist in the MODIS imagery that relate to the inversion layer water vapor gradient, which can not be directly measured using remote sensors. The water vapor gradient found within the inversion layer will determine if EM waves are trapped, creating a ducting region. Although there are often several regions in the atmosphere where ducts are created, this thesis will focus on the ducts created just above the stratocumulus-topped marine boundary layer found in the littoral regions and open oceans. This is a common occurrence found off the western coasts of mid-latitude continents during their summer months. Figure 1 illustrates the STBL for 21 July 2004 located off the west coast of California. This GOES-10 visual image was taken at 0000 UTC which corresponds to 1700 LT. Also shown on the image is the approximate location of the National Data Buoy Center (NDBC) buoy station 46011 in relationship to Vandenberg AFB. During this time of year, a semi-permanent high pressure system located over relatively cool air near the sea surface in eastern ocean basins create the stratocumulus boundary layer (STBL).

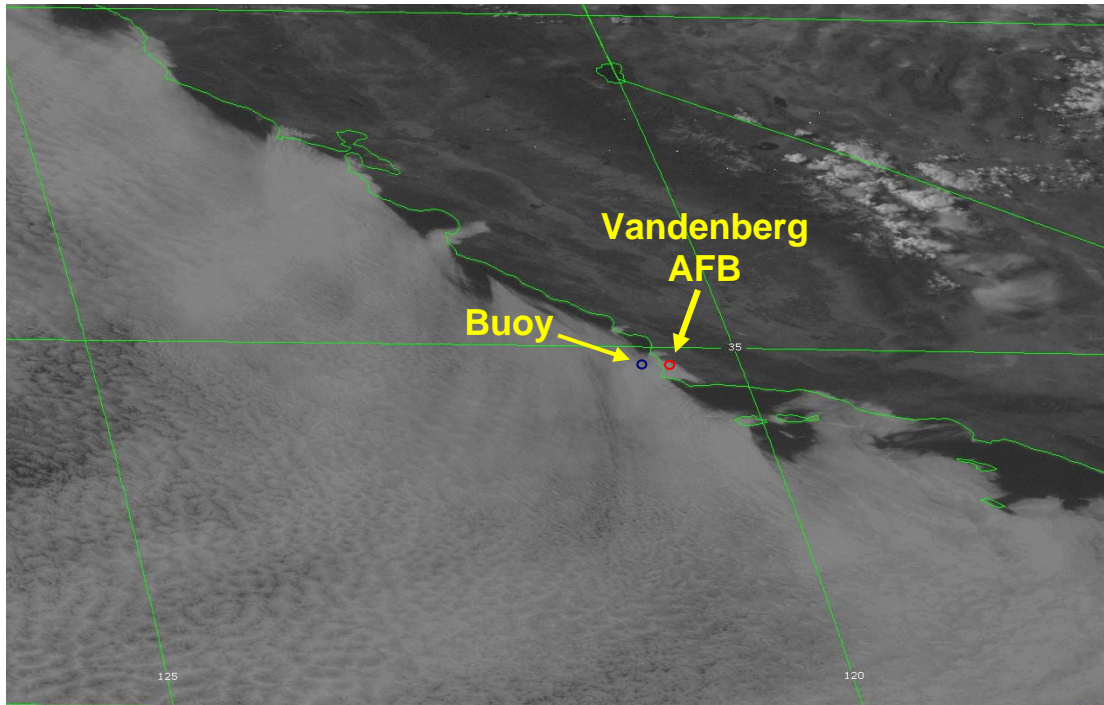


Fig. 1. GOES-10 visual image for 0000 UTC 21 July 2004. Example of the stratocumulus-topped marine boundary layer located off the Vandenberg coast and the approximate relationship between Vandenberg AFB and National Data Buoy Center (NDBC) buoy station 46011.

A screening process will be implemented to ensure that for each case there exists a well-defined stratocumulus cloud deck, as well as ensuring that there are no obstructions between the sensor and cloud tops to contaminate the measurements. Once the cases are screened, they will be inputted into the SEMEO program and compared to the Vandenberg soundings for validation.

Figure 2 represents regions in the world that are affected by this phenomenon called ducting. As illustrated by the highlighted areas of Fig. 2, almost anywhere on the globe that the US Navy would expect to operate has at least a 40% chance of experiencing the effects of ducts.

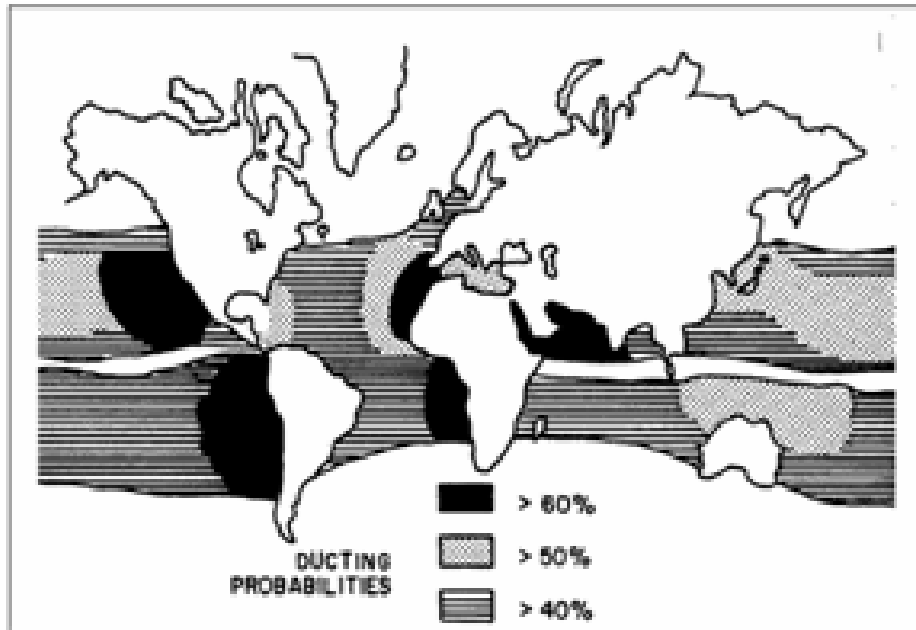


Fig. 2. World wide frequency of ducting occurrence. From Ortenburger et al (1985).

THIS PAGE INTENTIONALLY LEFT BLANK

II. THEORY

A. ELECTROMAGNETIC PROPAGATION THEORY

EM waves are divided into bands associated with frequency ranges. The bands are divided into groups that exhibit similar behavior. The frequency ranges that are most often affected by the observed atmospheric changes covered in this thesis are VHF (30-300MHz) and microwave frequencies which include UHF (0.3-3GHz), SHF (3-30GHz) and some EHF (30-300GHz) up to approximately 100GHz. These frequency ranges cover many RADAR and communication frequencies that are used today in both military and civilian applications. The atmospheric phenomenon that causes the electromagnetic waves to change course is refraction. Refraction is the property of the atmosphere that will cause the EM waves to bend from a straight line. This is a result of the changing air densities that the electromagnetic wave encounters as it propagates (Davidson 2005).

1. Index of Refraction, Refractivity, Modified Index of Refraction

The index of refraction (n) is related to the dielectric constant ϵ (where $n = \sqrt{\epsilon}$) and describes the interaction of the electric field of the EM wave with its medium. This index of refraction (n) is used to determine the phase speed along the EM wave front as it travels through the atmosphere. Since the value for the index of refraction (n) of VHF and microwave frequencies in air is very close to 1 (n_{air} typically has values from 1.0003 to 1.0005) it becomes convenient to define a new measure of refraction, called refractivity (N). Refractivity is based on how the index of refraction varies from one.

$$N = 10^6 (n-1) \quad (1)$$

Refractivity (N) is determined by the atmospheric temperature (T in degrees Kelvin), pressure (P in millibars) and water vapor pressure (e in millibars).

$$N = 77.6 P/T - 5.6 e/T + 3.73 \times 10^5 e/T^2 \quad (2)$$

The actual value of refractivity (N) is generally not important, but rather how its gradient, dN/dz , varies in the vertical. Using standard atmospheric conditions at sea level, the normal value of dN/dz is approximately -40km^{-1} . This would allow the EM wave to follow the standard radio horizon path. As the value of dN/dz becomes more positive, the EM waves will begin to sub-refract, which decreases the effective range of

the radar. Conversely, as the value of dN/dz becomes more negative, the EM propagation path will be super-refracted, increasing the effective radar's range. The sub-refractive, normal, and super-refractive propagation paths are illustrated in Fig. 3

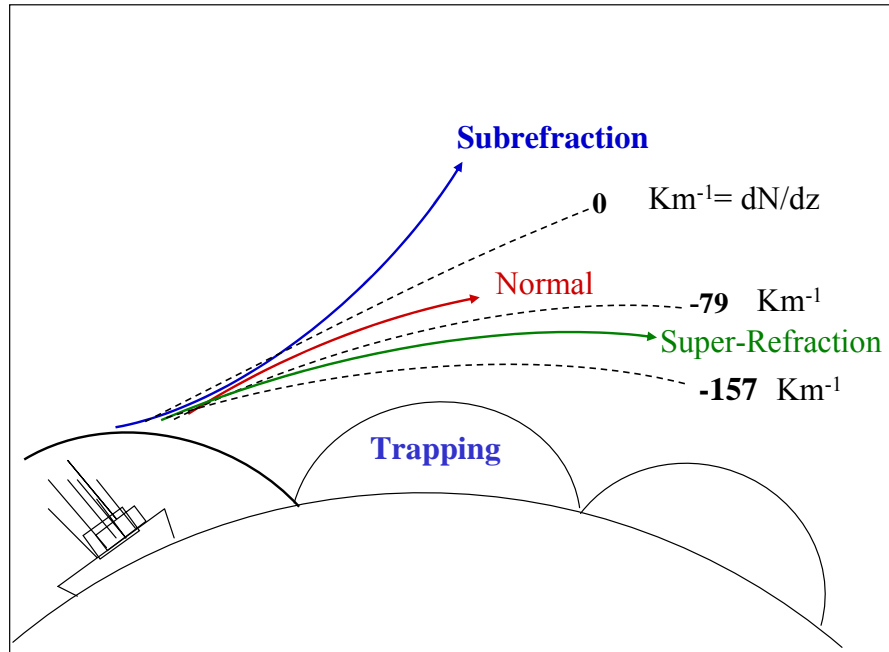


Fig. 3. Illustration of sub-refractive, normal, and super-refractive EM propagation categories and the associated gradient values of dN/dz . From Davidson (2005).

Figure 3 also illustrates the trapping region, occurring when $dN/dz < -157\text{km}^{-1}$. Trapping layers cause the EM waves to stay within a certain channel or duct for great distances. Identifying graphically where dN/dz is less than -157km^{-1} can be difficult, so a modification is made and referred to as the modified refractivity (M). The equation for M is similar to N; modified by the additional term of gradient (0.157m^{-1}) times altitude (Z) in meters.

$$M = N + (0.157\text{m}^{-1}) * Z \quad (3)$$

The modified index of refraction (M) profile allows one to clearly identify trapping/ducting regions in the atmosphere when looking at a graph of M versus altitude (Z). This is illustrated in Fig. 4 where the negative M gradient creates an elevated trapping layer and an elevated duct.

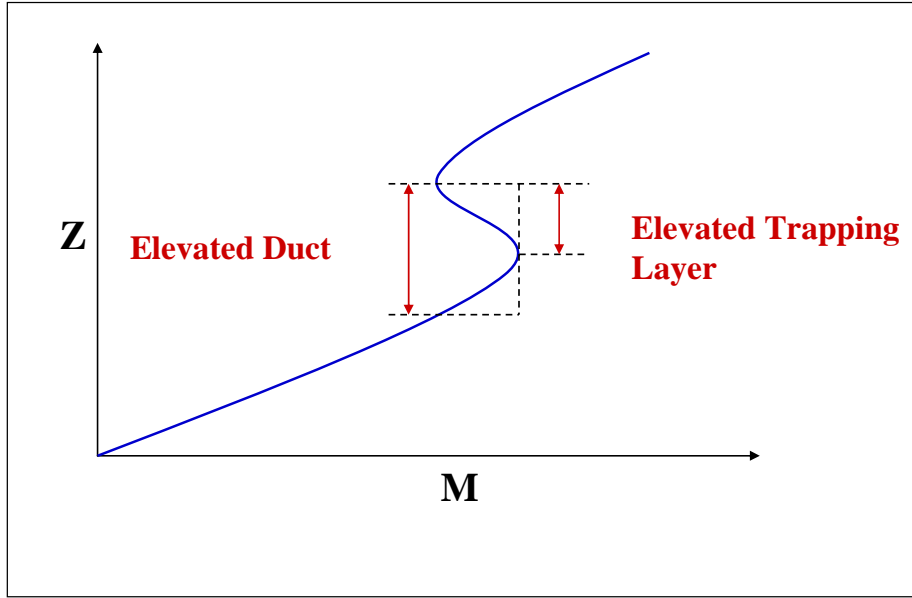


Fig. 4. Modified index of refraction (M) profile vs height (Z), illustrating the trapping layer created when the M gradient is negative. From Davidson (2005).

The modified refractive index (M) will be used in the rest of this thesis to depict regions of trapping graphically. Table 1 shows the numerical relationship between N and M gradients for current operational classifications and the resulting effect that would be expected from EM propagation.

Table 1. Numerical values associated with classes of refractivity. From Davidson (2005).

Classification	$\frac{dN}{dZ}$	$\frac{dM}{dZ}$	Distance to Surface Horizon
Sub-refraction	$> 0 \text{ km}^{-1}$		Reduced
Normal	$0 \text{ to } -79 \text{ km}^{-1}$	$> 157 \text{ km}^{-1}$	Normal
Super-refraction	$-79 \text{ km}^{-1} \text{ to } -157 \text{ km}^{-1}$	$0 \text{ to } 79 \text{ km}^{-1}$	Increased
Trapping	$< -157 \text{ km}^{-1}$	$< 0 \text{ km}^{-1}$	Greatly Increased

2. Definition of Trapping Layers and Ducts

Figure 5 illustrates the definition of a trapping layer (red), and its associated ducting layer (combined red and yellow layers). Figure 5 is an example of an elevated trapping layer and elevated duct, which is one of the three types of ducts that will be explained below. A trapping layer occurs in a layer where dM/dz is negative. A duct is the region in the M profile that is bounded at the top by the top of the trapping layer, and extends downward until it either intersects with the M profile or the surface.

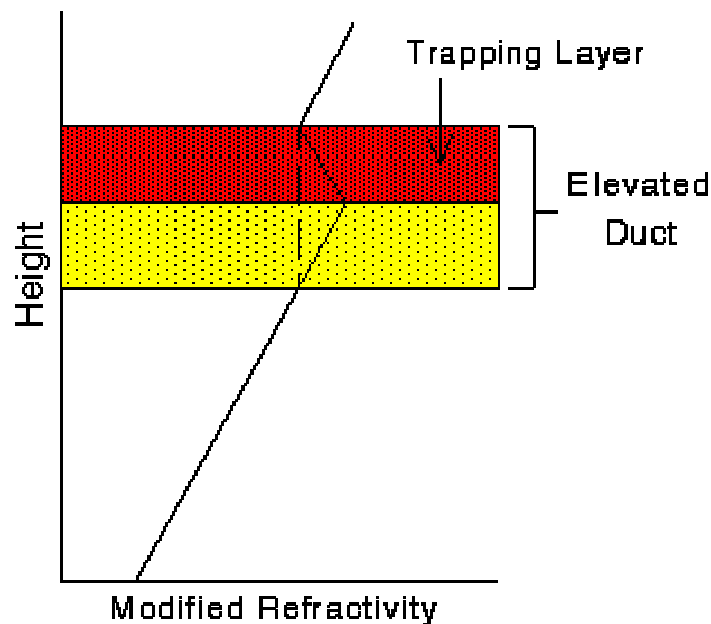


Fig. 5. Definition of a trapping layer and its corresponding duct. The red layer indicates where the M gradient is negative, which corresponds with the trapping region. The combined yellow and red layers identify the resulting duct.

3. Formation of Ducts

There are two mechanisms that generate ducts. The first is a result of the rapid vertical decrease in water vapor pressure found just above the oceans surface. The second mechanism is a result of the temperature and moisture gradients found within inversion layers. Based on these two mechanisms, three different types of ducts are characterized when dM/dz is negative, and are illustrated in Fig. 6. The blue line indicates the elevated duct, the red line describes the surface based duct, and the evaporative duct is the layer of negative dM/dz just above the surface. The evaporative

duct occurs near the oceans surface typically at depths between 2-30 meters and is a result of the first mechanism described. Because evaporative ducts occur over such a small region in the vertical, radiosondes are unable to represent them. The elevated duct generally occurs much higher than the evaporative duct and is a result of the second mechanism described. The elevated duct does not reach the surface while the surface based duct extends downward to the surface.

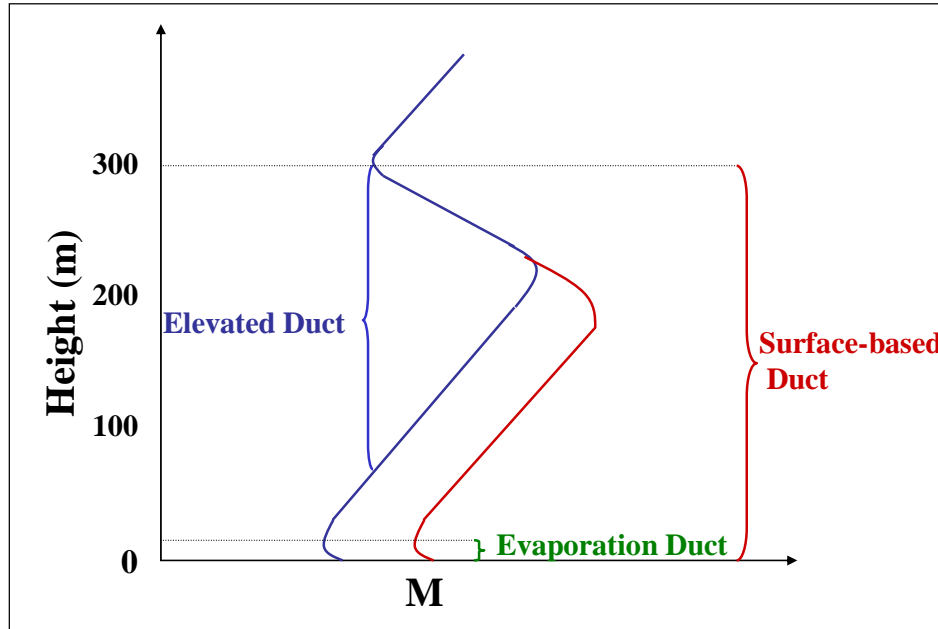


Fig. 6. Three different types of ducts: blue indicates the elevated duct, red is the surface based duct, and green in the evaporative duct. From Davidson (2005).

The surface-based duct is of particular interest in naval operations due to its correlation with radar antenna heights. Based on a radar antenna height of 20 meters, the radio horizon would be approximately 18.44 kilometers. This was computed using the following equation (AMS 2006)

$$R = \sqrt{17h}, \tag{4}$$

where R is the radio horizon in kilometers and h is the height of the antenna above the surface in meters. Figure 7 illustrates the significant increase in range that exists when a surface based duct is present. Notice that the evaporative duct on the left indicates radar

ranges out to approximately 30km, while the surface-based duct on the right extends radar ranges well beyond 200km.

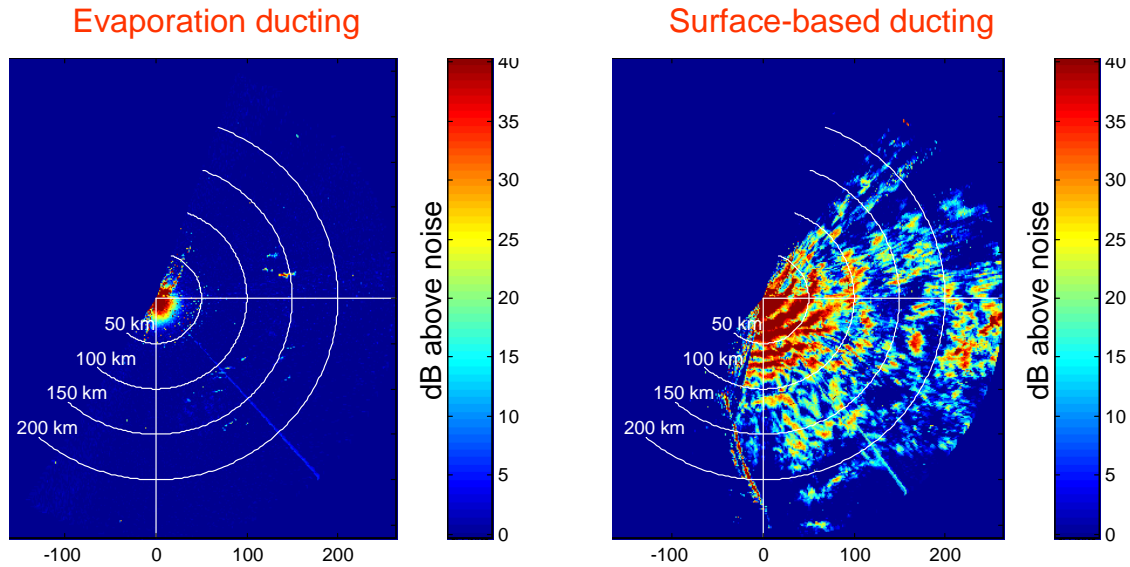


Fig. 7. Radar return within an evaporation duct (left) and an elevated surface-based duct (right). From Rogers (1999).

4. Frequency Dependence on Duct Size

As previously stated, whether an EM wave will be trapped is largely dependent on its frequency. This is because the wavelength has to be able to fit within the duct in order to be trapped. Figure 8 shows that as frequency increases (wavelength decreases), the depth of the duct required to trap that frequency decreases. Additionally, Table 2 illustrates some of the common frequencies used and the associated duct depths required for them to be trapped.

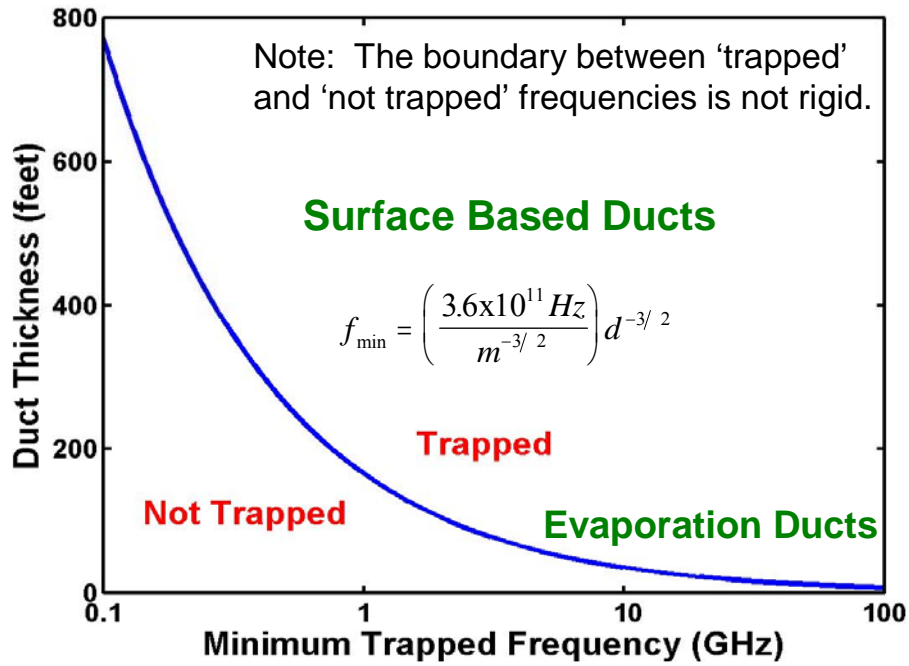


Fig. 8. Duct thickness required to trap radar frequencies between 0.1 to 100 GHz. From Davidson (2005).

Table 2. VHF and UHF radar bands and their required duct thickness to be trapped. From Davidson (2005).

Minimum Trapped Frequency (MHz)	Maximum Trapped Wavelength	Radar (Radio) Band	Duct Thickness	
			feet	meters
150	2.0 m	A (VHF)	587	179.0
192	1.56 m	A (VHF)	499	152.0
220	1.36 m	A (TAC UHF)	453	138.0
425	70.6 cm	B (TAC UHF)	294	89.6
1000	30.0 cm	D	166	50.6
3000	10.0 cm	F	80	24.3
5800	5.2 cm	G	51	15.6
8500	3.5 cm	I	40	12.2
9600	3.1 cm	I	37	11.2
10250	2.9 cm	J	35	10.7
15000	2.0 cm	J	27	8.3
30000	1.0 cm	K	17	5.24

B. CLOUD-TOP TEMPERATURE RETRIEVAL

One of the critical aspects of SEMEO is an accurate cloud-top temperature measurement. This is accomplished by understanding what photons the satellite sensor is measuring and where they are coming from. Assuming the cloud being sensed is optically thick, and that there is no interference above the cloud top that will affect the wavelengths being used to measure its temperature, then the spectral radiance measured by the sensor will be governed by simplifying the below Schwartzchild's equation.

$$L_t(\lambda, \theta, \varphi) = \varepsilon_s(\lambda, \theta)B(\lambda, T_s)\tau_d(\lambda) + \int_{p_0}^0 B(\lambda, T(p))\frac{d\tau_d(\lambda, p)}{dp}dp \quad (5)$$

L_t is the total spectral radiance measured at the top of the atmosphere as a function of wavelength (λ) and direction (θ, φ). Term one on the right hand side of Eq. (5) represents the emitted radiance from the surface as a function of wavelength and surface temperature. In the stratocumulus-topped marine boundary layer regions that this thesis is focused on, this term will go to zero. The reason for this is that within the IR wavelengths that are used to determine cloud-top temperature, the optically thick cloud will absorb all of the surface emitted energy, allowing none of the radiance to reach the cloud top. The integral represents the radiance emitted by the atmosphere from the surface to the top of the atmosphere where pressure equals zero. Since the integral only has value in a thin layer (typically less than 10m) at the cloud top, the integrand reduces to the Planck function for a blackbody $B(\lambda, T(p))$ where $T(p)$ is the temperature at the cloud top, T_{CT} . This now allows the original formula to be reduced to the following equation.

$$L_t(\lambda, \theta, \varphi) = B(\lambda, T_{CT}) \quad (6)$$

The Planck blackbody emittance is a function of wavelength and temperature at a certain pressure level. Since $L_t(\lambda, \theta, \varphi)$ is known, based on the results measured by the satellite, Eq. (6) can be solved for T_{CT} .

For the GOES-10 sensor, cloud-top temperature is determined from channel 4, which receives energy between 10.2-11.2 μ m. For the MODIS sensor, channel 31

(11.770-12.270 μm) is used. These wavelengths are ideal for measuring surface or cloud-top radiance values due to the lack of gaseous absorption in the atmosphere at these wavelengths (Kidder and Vonder Haar, 1995). Figure 9 provides a graphical representation of the percent of atmospheric transmission as a function of wavelength.

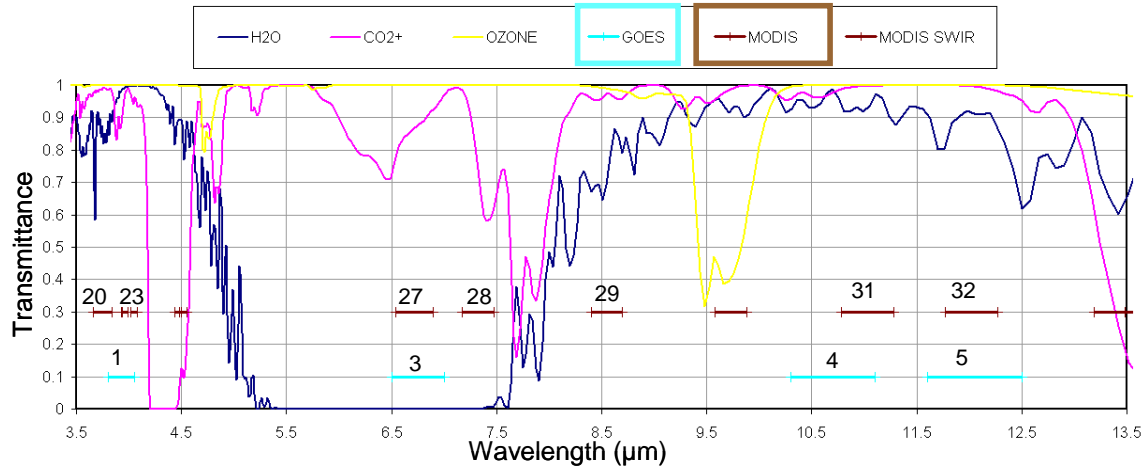


Fig. 9. Atmospheric transmittance for wavelengths 3.5-13.5 μm . Transmittance is reduced due to absorption by H₂O (blue), CO₂ (magenta) and ozone (yellow) gases. The spectral width of the GOES (light blue) and MODIS (brown) channels used in this thesis are indicated. From Durkee (2005).

C. ALGORITHM TO ESTIMATE CLOUD-TOP HEIGHT

SEMEO estimates the cloud top height based on knowledge of SST and cloud-top brightness temperature. The development of this technique was originally described in McBride (2000). The assumptions required to determine an accurate cloud-top height are:

1. Boundary layer is well mixed.
2. The air-sea temperature difference is small.
3. The percentage of the boundary layer depth which contains cloud (vertical cloud fraction) is dependent on the boundary layer depth.
 - Deep boundary layer (> 400m): top 1/3 is cloud, bottom 2/3 cloud-free.
 - Shallow boundary layer (< 400m): top 2/3 is cloud, 1/3 is cloud-free.

Figure 10 illustrates the model. Surface temperature and satellite infrared cloud-top temperature are known values. The lifted condensation level (LCL) is the base of the

cloud. The dry adiabatic lapse rate is used in the cloud-free region and the pseudo-adiabatic lapse rate is used in cloud. The step by step procedures are as follows.

1. Define the temperature difference between the cloud-top and surface.

$$\Delta T = T_{ct} - T_s \quad (7)$$

2. Using the measured ΔT and the dry adiabatic lapse rate (-9.84 C/km), estimate the boundary layer depth with no clouds (all temperatures in $^{\circ}\text{C}$, lapse rates in $^{\circ}\text{C}/\text{m}$, heights in meters)

$$Z_{dry} = \Delta T / \Gamma_{dry} \quad (8)$$

3. Assuming a vertical cloud fraction of 1/3 (meaning 2/3 is cloud-free), compute the height of the cloud base for a 2/3 cloud-free boundary layer.

$$Z_{CloudBase} = 2/3 * Z_{dry} \quad (9)$$

4. Using the dry adiabatic lapse rate, Γ_{dry} , and the surface temperature, T_s , compute the cloud-base temperature for a 2/3 cloud-free boundary layer.

$$T_{CloudBase} = (\Gamma_{dry} * Z_{CloudBase}) + T_s \quad (10)$$

5. Using the measured cloud-top temperature, T_{CT} , the cloud-base temperature, $T_{CloudBase}$, and the pseudo-adiabatic lapse rate, Γ_{moist} (-7.0 $^{\circ}\text{C}/\text{km}$), compute the cloud depth (m).

$$CloudDepth = (T_{CT} - T_{CloudBase}) * \Gamma_{moist} \quad (11)$$

6. Compute the cloud-top height (m), $Z_{CloudTop}$, using the cloud-base height and cloud depth.

$$Z_{CloudTop} = Z_{CloudBase} + CloudDepth \quad (12)$$

7. If the cloud-top height is less than 400 meters, recompute the cloud-top height using an assumption of 2/3 vertical cloud fraction (meaning 1/3 is cloud-free). Use Eq. (9) with a cloud-free ratio of 1/3 vice 2/3. Using the new cloud-base height, use Eqs. (10)-(12) to generate a new, higher estimate of cloud-top height. The rationale for re-computing cloud-top height is that a shallow STBL typically has a greater vertical cloud fraction. The 400m break point was determined from observations by McBride (2000).

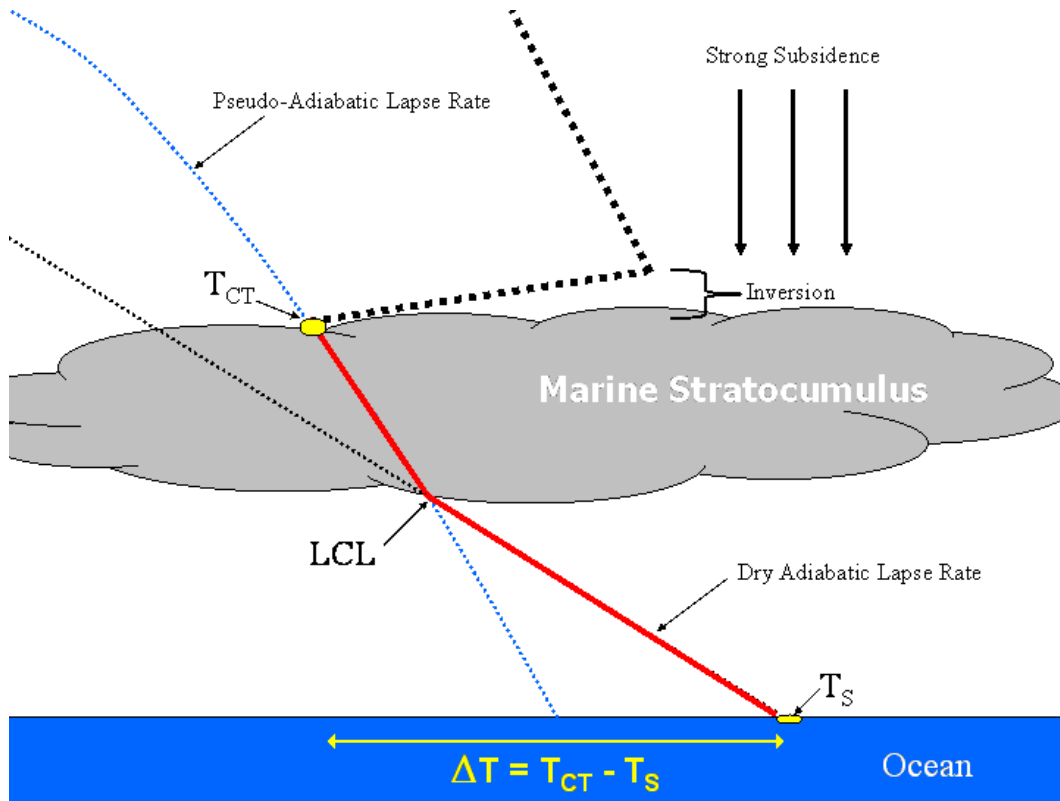


Fig. 10. Surface temperature (T_S) and satellite infrared cloud-top temperature (T_{CT}) are known values. The lifted condensation level (LCL) is the base of the cloud. The dry adiabatic lapse rate is used in the cloud-free region and the pseudo-adiabatic lapse rate is used in cloud. From Jordan and Durkee (2003).

D. ALGORITHM TO ESTIMATE DUCT STRENGTH AND DEPTH

The refractive profile below the inversion can be estimated using information derived in the SEMEO cloud-top height algorithm and numerical model estimates of surface pressure. A parameterization is included in SEMEO to estimate the modified refractive index through the inversion. The parameterization estimates the trapping layer strength (ΔM) and the trapping layer depth. When combined with the 850mb modified refractive index (computed from numerical model fields), the SEMEO process provides a five-point modified refractive index vertical profile, surface to 850mb.

The first component in the SEMEO process uses satellite-measured stratocumulus cloud infrared temperature, surface temperature, and assumptions about cloud fraction within the boundary layer, as described in Chapter 2, section C. Using numerical model estimates of surface pressure and relative humidity, and the hypsometric equation, the M

profile can be computed at three points: the surface, cloud base (LCL) and cloud top. The cloud-top height is the base of the trapping layer and also the height of the maximum M value within the trapping layer.

The second SEMEO component applies the refractive profile parameterization within the inversion to estimate the trapping layer strength (ΔM) and depth, which adds one point to the profile generated in the first step of SEMEO. The modified refractive index estimate at 850mb is the fifth point of the profile. Figure 11 compares a measured refractive profile with a five-point profile simulation of the SEMEO procedure.

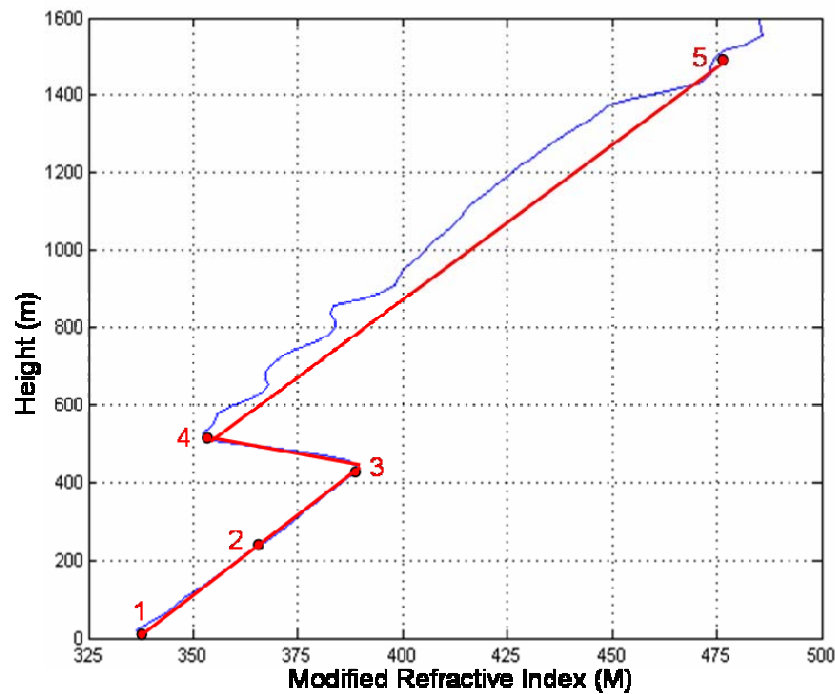


Fig. 11. Simulated five-point modified refractive index profile from the SEMEO procedure (red) is compared with the measured radiosonde (blue) from the MAST experiment, 21 June 1994. Points 1-3 are generated from the cloud-top height algorithm. Point 4 is from the trapping layer parameterization technique, and Point 5 is from numerical model estimates of 850mb fields.

The inversion moisture and temperature gradients above the STBL both contribute to the trapping layer strength, but the moisture gradient has the greatest

influence. While it is desirable to parameterize the moisture decrease, only the temperature increase in the inversion is parameterized in the first generation of SEMEO.

The temperature, $\Delta T'$, which is a parameterization of the temperature increase in the trapping layer, is computed using the 850mb temperature from each profile, which is warmed dry adiabatically from 850mb to the height of the inversion base. The parameterized temperature is computed:

$$\Delta T' = T_{850mb} + \frac{9.84C}{1000m} (Z_{850mb} - Z_{InversionBase}), \quad (13)$$

where Z indicates height (m). Figure 12 graphically illustrates this process.

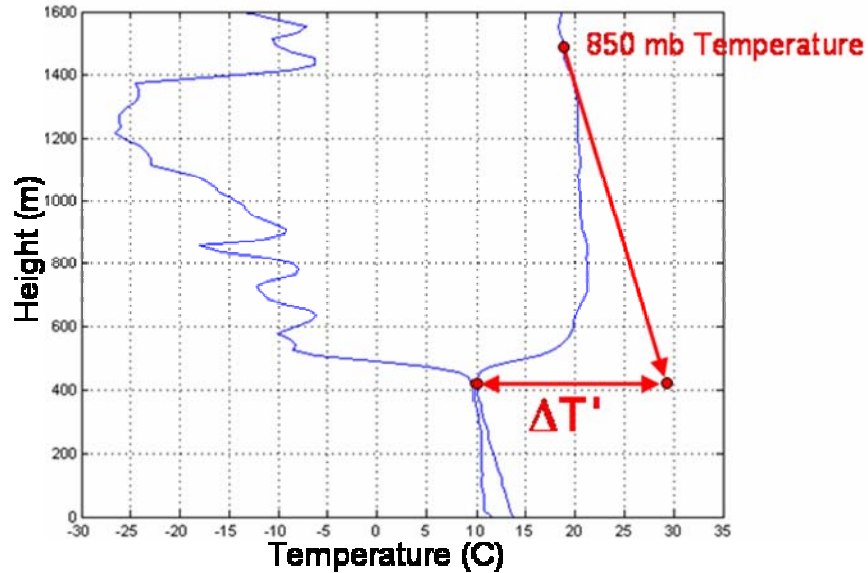


Fig. 12. Temperature, $\Delta T'$, which is a parameterization of the temperature increase in the inversion, is computed using the 850mb temperature from each profile, which is warmed dry adiabatically from 850mb to the height of the inversion base. The blue profile on the left represents the dewpoint temperature and the blue profile on the right represents the temperature profile.

The parameterized temperature, $\Delta T'$, is used to estimate the trapping layer strength (ΔM) for each profile using:

$$\Delta M = 1.1543 * \Delta T' + 4.71 \quad (14)$$

Eq. (14) is based on linear regression analysis of a different sounding dataset than used in this thesis. The trapping layer depth, is fixed at 100 meters within the algorithm, was determined from sounding statistics using the same dataset used for Eq. (14) (Jordan, 2006, personal communication)

The step by step procedures to generate the SEMEO refractive index profile are as follows:

1. Run the cloud-top height estimation algorithm. The output of the algorithm is a three-point vertical profile of temperature and height for the surface, LCL, and cloud top.
2. Estimate the surface value of modified refractive index (M) using the buoy-measured surface pressure, surface temperature and an estimated relative humidity value of 85%.
3. Use the hypsometric equation to estimate the pressure at the LCL using the surface pressure, the LCL height, and the average value of the surface and LCL temperatures.
4. Estimate M at the LCL using the LCL pressure, temperature, height, and relative humidity value of 100% (in cloud).
5. Use the hypsometric equation to estimate the pressure at the cloud top using LCL pressure, the cloud-top height, and the average temperature in the layer.
6. Estimate the cloud-top value of modified refractive index, M, using pressure, temperature and relative humidity value of 100% (in cloud).
7. Calculate the parameterized temperature, $\Delta T'$, using the radiosonde 850mb temperature and height, and the cloud-top height, Eq. (13).
8. Calculate the M strength, ΔM , using the refractivity parameterization (Eq. (14)).
9. Calculate the value of M at the top of the trapping layer:

$$M_{TopTrapping} = M_{CloudTop} - \Delta M \quad (15)$$

10. Calculate the height of the top of the trapping layer using a constant value of trapping layer depth, 100m (Eq. (16)).

$$Z_{TopTrapping} = Z_{CloudTop} + Z_{DepthTrappingLayer} \quad (16)$$

11. Calculate the value of M at 850mb using the radiosonde 850mb temperature, height and relative humidity. Assign the radiosonde 850mb height value to the fifth location in the height vertical profile.

THIS PAGE INTENTIONALLY LEFT BLANK

III. DATA AND PROCEDURES

A. INSTRUMENTS

1. Moderate Resolution Imaging Spectroradiometer (MODIS)

The MODIS instrument is a rotating scan mirror-type imager that is deployed aboard the Earth Observing System (EOS) satellites, Aqua and Terra. Both Aqua (launched May 2002) and Terra (launched late 1999) are polar-orbiting satellites with near-circular; sun-synchronous orbits with approximately 98.2 degrees of inclination at an altitude of approximately 705 km (Goddard Space Flight Center, 2003). Aqua's orbit is such that it ascends across the equator at about 1330 LT while Terra's orbit is such that it descends across the equator at about 1030 LT.

MODIS is a scanning imaging radiometer with a viewing swath width of 2330 kilometers. MODIS provides high-resolution images of daylight-reflected solar radiation and 24-hour thermal (IR) information over all regions of the globe. Its spatial resolution ranges from 250 meters (red channel only) to 1 kilometer (all IR channels). The broadband spectral coverage of the instrument (0.4 to 14.4 μm) is divided into 36 bands of various bandwidths optimized for imaging surface and atmospheric features. Due to the focus of this thesis, seven of these channels will be studied. They are channels 20, 23, 27, 28, 29, 31, and 32. The transmissivity characteristics of these channels were previously identified in Fig. 9. Table 3 lists all 36 channels.

Table 3. MODIS Channel Primary Use and Specifications. (Adapted from GSFC 2003).

Primary Use	Band	Bandwidth ¹	Spatial Resolution ²	Spectral Radiance ³	Required SNR ⁴
Land/Cloud/Aerosols Boundaries	1	620 - 670	250	21.8	128
	2	841 - 876	250	24.7	201
Land/Cloud/Aerosols Properties	3	459 - 479	500	35.3	243
	4	545 - 565	500	29.0	228
	5	1230 - 1250	500	5.4	74
	6	1628 - 1652	500	7.3	275
	7	2105 - 2155	500	1.0	110
Ocean Color/Phytoplankton/Biogeochemistry	8	405 - 420	1000	44.9	880
	9	438 - 448	1000	41.9	838
	10	483 - 493	1000	32.1	802
	11	526 - 536	1000	27.9	754
	12	546 - 556	1000	21.0	750
	13	662 - 672	1000	9.5	910
	14	673 - 683	1000	8.7	1087
	15	743 - 753	1000	10.2	586
	16	862 - 877	1000	6.2	516
Atmospheric Water Vapor	17	890 - 920	1000	10.0	167
	18	931 - 941	1000	3.6	57
	19	915 - 965	1000	15.0	250
<hr/>					
Primary Use	Band	Bandwidth ¹	Spatial Resolution ²	Spectral Radiance ²	Required NE[delta]T(K) ⁴
Surface/Cloud Temperature	20	3.660 - 3.840	1000	0.45(300K)	0.05
	21	3.929 - 3.989	1000	2.38(335K)	2.00
	22	3.929 - 3.989	1000	0.67(300K)	0.07
	23	4.020 - 4.080	1000	0.79(300K)	0.07
Atmospheric Temperature	24	4.433 - 4.498	1000	0.17(250K)	0.25
	25	4.482 - 4.549	1000	0.59(275K)	0.25
Cirrus Clouds Water Vapor	26	1.360 - 1.390	1000	6.00	150(SNR)
	27	6.535 - 6.895	1000	1.16(240K)	0.25
	28	7.175 - 7.475	1000	2.18(250K)	0.25
Cloud Properties	29	8.400 - 8.700	1000	9.58(300K)	0.05
Ozone	30	9.580 - 9.880	1000	3.69(250K)	0.25
Surface/Cloud Temperature	31	10.780 - 11.280	1000	9.55(300K)	0.05
	32	11.770 - 12.270	1000	8.94(300K)	0.05
Cloud Top Altitude	33	13.185 - 13.485	1000	4.52(260K)	0.25
	34	13.485 - 13.785	1000	3.76(250K)	0.25
	35	13.785 - 14.085	1000	3.11(240K)	0.25
	36	14.085 - 14.385	1000	2.08(220K)	0.35
<hr/>					
¹ Bands 1 to 19 are in nm; Bands 20 to 36 are in μm ² Resolution at nadir in meters ³ Spectral Radiance values are ($\text{W}/\text{m}^2 \cdot \mu\text{m}\cdot\text{sr}$) ⁴ SNR = Signal-to-noise ratio ⁵ NE(delta)T = Noise-equivalent temperature difference					

2. Geostationary Operational Environmental Satellite (GOES)

The United States normally operates two meteorological satellites in geostationary orbit over the equator. GOES-10 (or GOES-West) was launched on 25 April 1997 and positioned over the equator at 135W longitude. GOES-12 (or GOES-East) was launched on 23 July 2001 and was positioned over the equator at 75W longitude. Both satellites are in a geosynchronous orbit about 35,800km (22,300 miles) above the earth. Both the altitude and longitude of GOES-10 permits it to have continuous coverage of the West coast of the United States and the Pacific Ocean. The GOES-10 imager was used to provide images and brightness temperature values which were compared against the aforementioned MODIS sensor. Three of the five image channels shown in Table 4 were used in this study; they are channels 1, 2, and 3.

Table 4. GOES-10 and GOES 12 Imager

Band	Wavelength Region (μm)	Resolution (km)
1	0.65 (green-red)	1
2	3.9 (Mid-wave Infrared)	4
3	6.7 (Thermal Infrared)	8
4	11 (Thermal Infrared)	4
5	12 (Thermal Infrared)	4

3. Atmosphere Profile Measurements

The microsondes used at Vandenberg AFB to measure the temperature and humidity profiles during the time period of interest were GPS MARK II model 610 and 710 manufactured by Lockheed Martin Sippican (L. Wells, Vandenberg AFB, 2006, personal communication). These microsondes sample the pressure, temperature, humidity, and winds once per second. The data is then digitally transmitted twice, for added reliability, at a transmission rate of 9600 baud. The FM transmission frequency is 1 of 16 discrete frequencies chosen before launch within a range of 400-406MHz. The pressure sensor is a continuously variable capacitance aneroid type. The pressure range

is 1080mb to 3mb with an accuracy of ± 0.5 mb (rms) and a resolution of 0.1mb. Temperature is measured via a resistive type chip thermistor which has a reflective coating that minimizes errors due to solar and infrared radiation effects. The temperature range is $+60^{\circ}\text{C}$ to -90°C with an accuracy of $\pm 0.2^{\circ}\text{C}$ (rms) and a resolution of 0.1°C . The humidity sensor is a carbon type with a range of 5 to 100% RH; within $+40^{\circ}\text{C}$ to -50°C . The accuracy of the humidity sensor is 2% RH (rms) with a 1% RH resolution. Accurate winds are derived from the GPS satellite network. Additionally, geopotential height is calculated directly from altitude measured with code-correlating differential GPS which provides greater accuracy than the traditional calculation method made from pressure, temperature and humidity (T. Curran, Lockheed Martin Sippican, 2006, personal communication).

The microsondes were all launched at standard synoptic times, 0000 UTC and 1200 UTC, from Vandenberg Air Force Base (VAFB), home of the 30th Space Wing. VAFB is located along the central coast of California approximately halfway between Los Angeles and San Francisco, 55 miles northwest of Santa Barbara.

The location of the launch site is $34^{\circ} 45' 12.7520''\text{N}$ and $120^{\circ} 34' 15.8610''\text{W}$ and is approximately 111m above sea level and approximately 3.75 miles inland. There is a gradual slope downward from the launch site to the ocean with no obstructions between the launch site and the ocean (L. Wells, 30 WS/SYR, 2006, personal communication). Although the stratocumulus-topped marine boundary layer is most prevalent in the summer months, this study included all available soundings between the months of April through October. The associated years were 2003-05 for the aforementioned months, and April and May of 2006. A total of 1297 soundings were reviewed, of which 93% contained a duct at or above the STBL. After reviewing the soundings, they were separated into 3 categories based on the duct characteristics described below.

4. Sea Surface Temperature (SST) Data

Sea surface temperature data was available from buoy station 46011. Station 46011 is a 3-meter discus buoy located at 34.88N and 120.87W . Station 46011 is owned and maintained by the National Data Buoy Center (NDBC) which is branch of the National Oceanic and Atmospheric Administration (NOAA). At approximately 20 miles west-northwest, station 46011 was the closest buoy location to the Vandenberg launch

site. Station 46011 is located in a water depth of 188.4m and collects hourly measurements of multiple atmospheric and oceanographic data. For the purpose of this thesis, the sea surface temperature and air temperature were collected. The sea surface temperature is measured at a depth of 0.6m below the surface and the air temperature is measured at a height of 4m above the surface.

B. PROCEDURES

1. Categorizing the Soundings

The first step is to compute modified refractivity (Eq. 3) to create an M profile for each of the 1297 soundings that were considered in this study. Modified refractivity was computed from the reported sounding values; no quality control was performed. Once the M profiles were generated, further analysis was focused on the refractive region just above the STBL.

Of the 1297 soundings observed, there were 85 soundings that did not indicate a negative M gradient whatsoever, and therefore gave no indication of any refractive layer(s) within the soundings profile. Of the 85 duct-free soundings, only 9 of them occurred in the months of June, July, or August. This highlights the tendency that the ducting phenomenon preferentially occurs in the summer months off the coast near Vandenberg. Additionally, soundings that indicated a very high relative humidity signature throughout most of the troposphere were excluded from further analysis. This was based on the upper-level moisture preventing the satellite sensors from obtaining accurate cloud-top measurements.

Based on the generated M profiles, analysis was focused on the temperature and dewpoint temperature gradients within the trapping layer. The objective was to note how much of a difference in both temperature, and dewpoint temperature was realized in the trapping region of the M profile. The focus of this analysis within the trapping layer was based on the refractive equation, Eq. (3), and the significance placed on the gradients of temperature and dewpoint temperature in determining regions and strength of refractivity. These results were the basis for dividing the soundings into 3 categories.

Category 1 represented those soundings that had a similar difference in both the temperature and the dewpoint temperature within the identified trapping region. Additionally these cases were screened to ensure there were no indications of saturated regions above the targeted inversion layer that would prevent the satellite from being able to get an accurate cloud top temperature. Figure 13 is an example of a Category 1 profile.

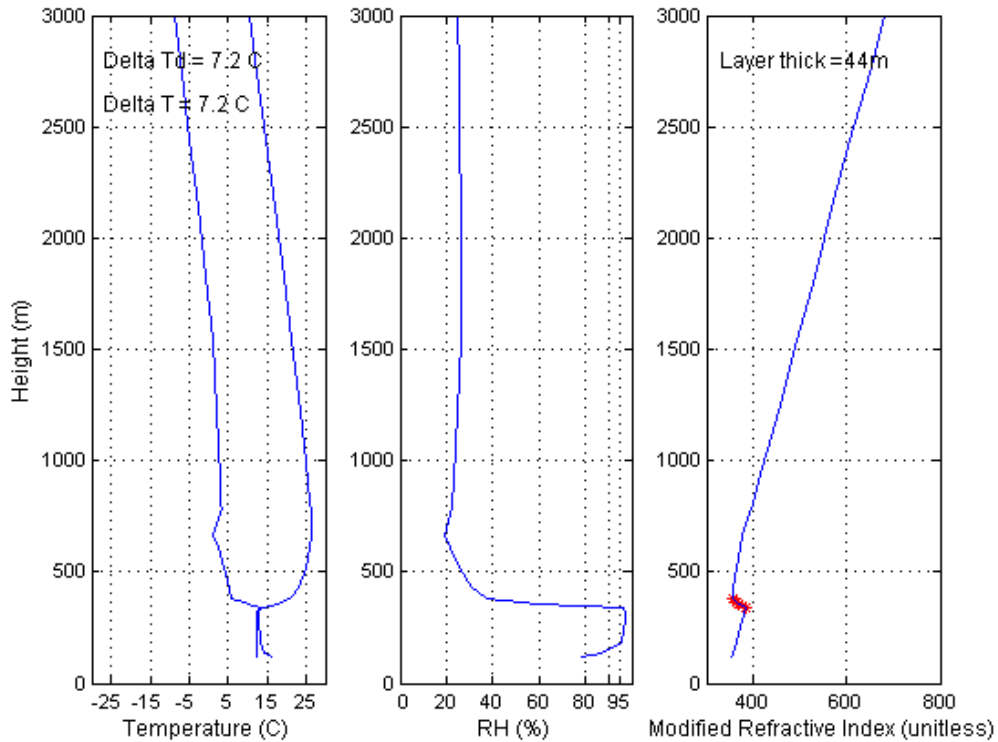


Fig. 13. Example of a Category 1 profile where the magnitude of the gradient for both temperature and dewpoint temperature within the identified trapping layer are similar. Here they both experience a 7.2 °C change. This sounding was launched on 0000 UTC 25 September 2004.

Category 2 represents those soundings with the magnitude of the temperature difference averaging at least twice the dewpoint temperature difference within the trapping region. As before, these cases were screened to ensure there were no saturated regions above the targeted inversion layer to prevent an accurate cloud-top temperature measurement. Figure 14 is an example of a Category 2 profile.

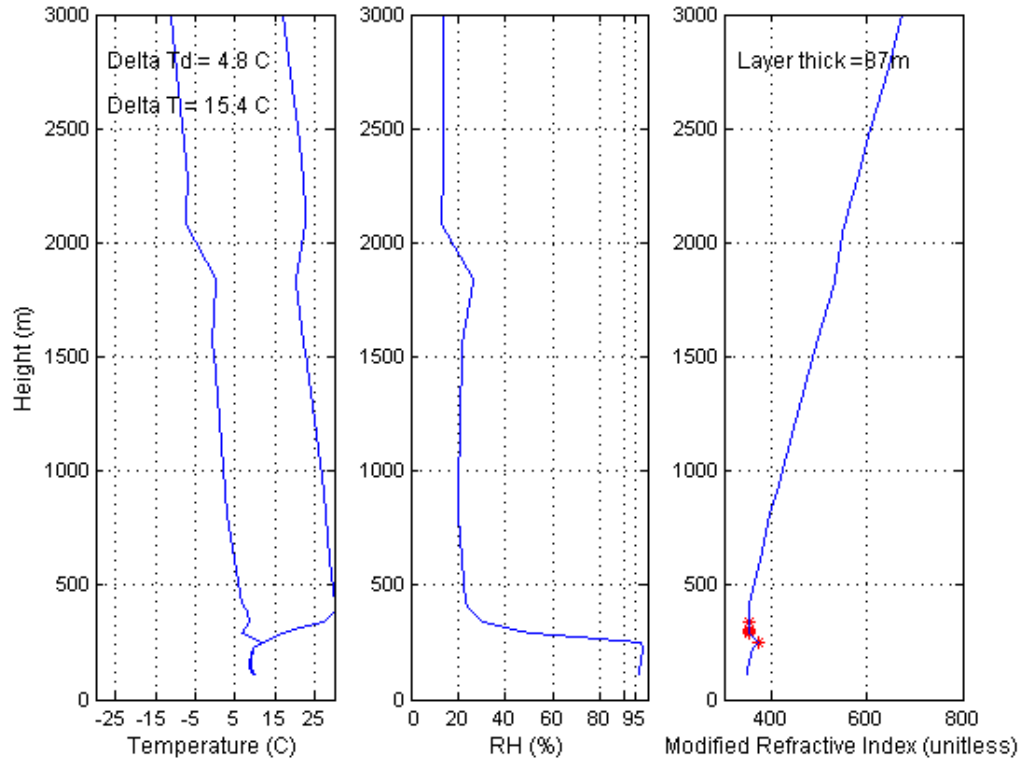


Fig. 14. Example of a Category 2 profile where the average difference in temperature is at least twice the dewpoint temperature difference within the identified trapping region. Here the temperature difference was 15.4°C and the dewpoint temperature difference was 4.8°C . This sounding was launched on 1200 UTC 11 July 2003.

Category 3 represents those soundings that had a dewpoint temperature difference at least twice that of the temperature difference within the targeted trapping region. Of note, Category 3 represented the majority of the soundings in the Vandenberg dataset and the dewpoint temperature difference was generally much more than twice the temperature difference, as seen in Table 5. These cases were also screened to ensure saturated regions above the targeted inversion layer did not exist. Figure 15 is an example of a Category 3 profile.

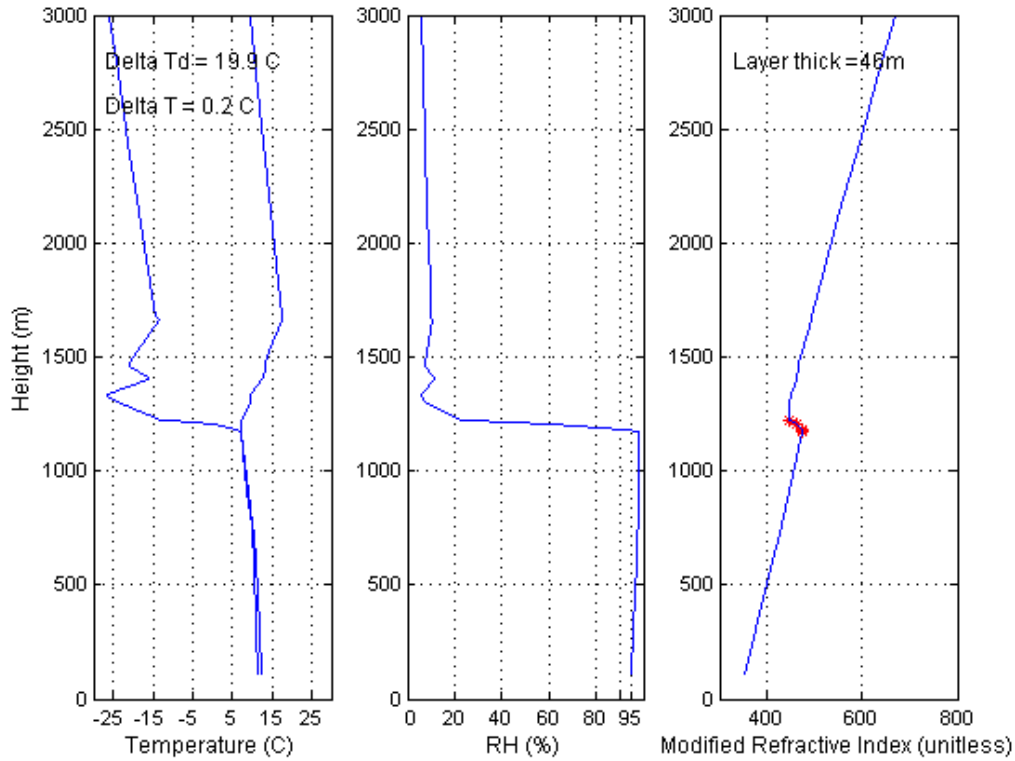


Fig. 15. Example of a Category 3 profile where the difference in dewpoint temperature is at least twice the temperature difference within the targeted trapping layer. Here the dewpoint temperature difference was 19.9°C and the temperature difference was 0.2°C . This sounding was launched on 1200 UTC 10 June 2003.

Table 5 presents the statistics from the 1212 Vandenberg AFB sounding with elevated trapping layers. These statistics are based on the first elevated trapping layer; evaporative ducts are excluded. This trapping region was located at the top of the STBL and was a result of the inversion located at the cloud top. Many soundings had additional negative refractive layers higher in the troposphere, but were not the focus of this thesis and were not included in the statistics.

Table 5. Statistics for the first elevated trapping layer (top of STBL) for the 1212 Vandenberg soundings with a negative M gradient. Soundings included are from Apr-Oct 2003-05, and Apr-May 2006.

	Average	Standard Deviation
Trapping layer depth (m)	72.0	48.6
Duct thickness (m)	165.0	123.5
Height (m) of the base of the trapping layer	632.0	629.0
Dewpoint temperature difference (C) within the trapping layer	7.9	7.5
Temperature difference (C) within the trapping layer	2.6	4.0
M difference, ΔM , (unitless) within the trapping layer	14.4	17.3

Capturing the exact inversion structure above the STBL may be difficult with the standard radiosonde reporting. For some vertical profiles, dewpoint temperature measurements unexpectedly continued to increase while the coincident air temperature increased, as expected, in the inversion. One possible explanation is the humidity sensor response time and the amount of time it takes the sensor to dry off after exiting the cloud top. As the sensor ascends through the cloud and then abruptly enters a drier region in the temperature inversion, there may be a time lag while the humidity sensor is drying before it can then report accurately. Within this region (generally less than 100 meters) some profiles indicate dewpoint temperature measurements continuing to increase in concert with the temperature increase.

Figure 16 is an example of dewpoint temperature measurements continuing to increase after the temperature inversion. By not responding accurately, the resulting M profile (on the right) misrepresents a trapping region.

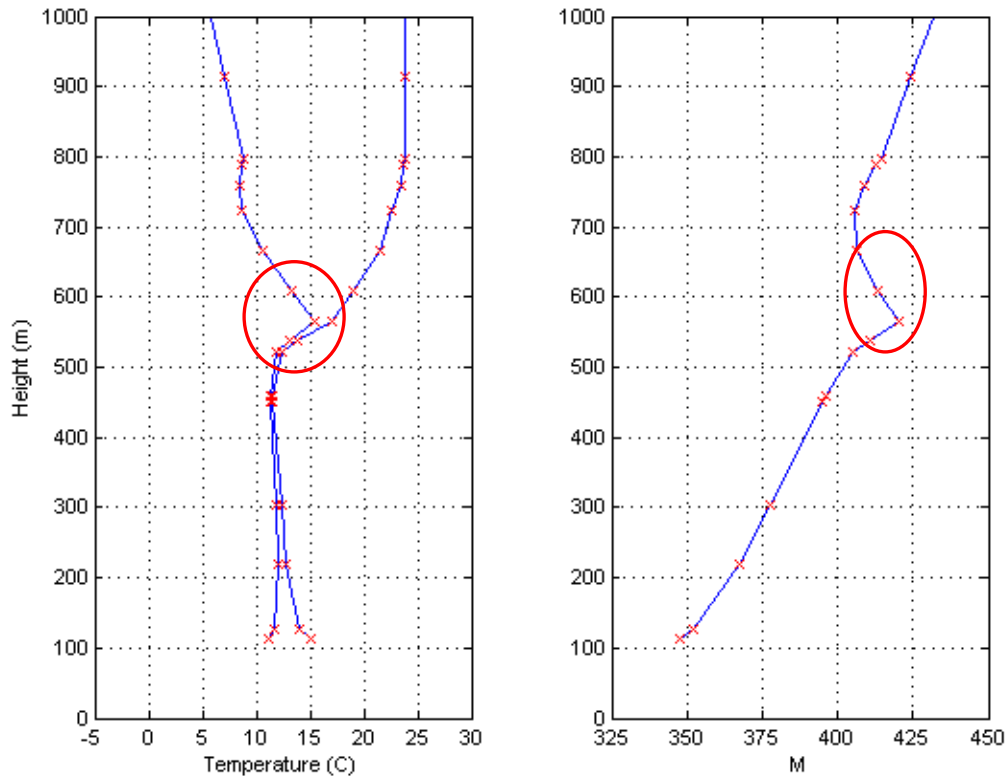


Fig. 16. Example of possible erroneous dewpoint temperature values. The cloud top occurs at 521m, yet dewpoint temperature continues to increase for 100 meters. In the 100m layer, relative humidity and M values are assumed to be in error. This sounding was launched at 0000 UTC 31 August 2003.

The final step was to choose cases within the above described categories to further analyze with MODIS and GOES imagery. Based on the limited number of Category 1 and 2 cases, 15 cases from each category were set aside for further analyzed.

2. MODIS and GOES Images

The GOES visible, infrared, and water vapor images that were temporarily and spatially coincident with the selected 45 cases were analyzed next. These images were available online through the Comprehensive Large Array data Stewardship System (CLASS) of the NOAA Satellite and Information Service. When visible images were available, they were examined to understand the integrity of the STBL over the region of interest. The concern here was that if thin or broken stratus was observed, then cloud top measurements may not be accurate due to photons from the surface contaminating the cloud top brightness temperature results. The infrared images were available for all cases

and were examined next. These images provided additional support for the density of the STBL as well as noting if there was any evidence of cirrus aloft. Cirrus aloft can result in the brightness temperature measurements being colder than would be expected since the measured radiance originates from much higher in the atmosphere. Finally the water vapor images provided an overall understanding of the surrounding pattern, troughing or ridging aloft, as well as indicating whether or not the area of interest was in a “dry” or “moist” region of the water vapor pattern.

MODIS images were also available online from the Distributed Active Archive Center (DAAC). MODIS images were selected based on image coverage of Vandenberg AFB and the closest match of satellite overpass and sounding launch time (synoptic times). For the cases in this thesis, the Aqua sensor provided the most accurate temporal match. As mentioned above, and illustrated in Fig. 9, the channels that were then analyzed were channels 20, 23, 27, 28, 29, 31, and 32. Channels, 20 and 23, fall within a region of the electromagnetic spectrum that can receive energy from both earth and cloud emissions as well as reflected solar irradiance. Channels 27 and 28 receive energy primarily from the mid to upper troposphere between 300mb and 600mb. Cirrus clouds, the water vapor concentrations, and the dynamic flow pattern can be readily identified with channels 27 and 28. Channel 29 allows for identification of cloud properties. Channels 31 and 32 are used to collect cloud-top temperature measurements.

3. MODIS and GOES Comparisons

MODIS imagery has higher spatial and radiometric resolution than GOES imagery. Assuming that MODIS channel 31 brightness temperatures are more accurate than GOES channel 4, a test was conducted to determine if and how much of a difference occurs. This is necessary because the GOES channel 4 measurements are used in the SEMEO program to estimate cloud-top height. Before the test could be conducted, the GOES imagery that best matched the MODIS overpass time was obtained. The bias between MODIS and GOES was determined using 9 of the final 30 cases based on the following criteria.

Using the GOES channel 4 brightness temperatures over buoy 46011, a comparison was made between the cloud-top brightness temperatures at sounding launch time and the GOES temperature for the image nearest to the MODIS pass time. If there

was no difference between the two GOES brightness temperature values, then these cases were set aside for further evaluation. The purpose of this step was to indicate how the stratus deck was changing with time over the buoy location. This was necessary because the MODIS and GOES values used to determine the bias are not exactly time coincident, but generally within 10 minutes. This gave additional confidence to the comparison when it was evident that the stratus deck had not changed over the 2-3 hours difference between the MODIS pass time and the sounding time.

The MODIS footprint was evaluated next. This was to ensure that the buoy location was well within the field of view of the MODIS sensor which provided confidence in the brightness temperature values received. If the buoy was located near the edge of the MODIS pass, that case was discarded.

Next, the evaluation of the visible and IR images from MODIS and GOES was conducted. Cases were removed from further evaluation during this process if the images indicated regions of cirrus aloft, or if there were thin or broken stratus clouds over the region of interest (i.e, buoy location). If cirrus was present, then the brightness temperature values would be colder because the photons being measured were from higher in the atmosphere. If thin or broken clouds were present, then warmer brightness temperatures would be measured because of the photons sensed would be from lower in the atmosphere.

Once the nine cases were identified, the cloud-top brightness temperature values from GOES channel 4 were subtracted from those found with MODIS channel 31. For the nine cases identified, a varying amount of positive difference was observed for all cases. The average difference was 0.34°C. Correction for this bias was not used in the SEMEO computations. This decision was based on the following. To be reliable, the source of this bias must be confirmed. In this case, the differences between MODIS and GOES measurements could have resulted from sensor spectral response, spatial resolution (1 km vs 4 km), and view geometry differences.

Table 6. Nine cases used to determine if a bias exists between MODIS and GOES brightness temperatures.

Date	MODIS Pass Time (UTC)	MODIS Ch. 31 Brightness Temperature (C)	GOES Pass Time (UTC)	GOES Ch. 4 Brightness Temperature (C)	Difference, MODIS-GOES, (C)
22 May 2003	2040	9.57	2045	9.40	0.17
11 Jul 2003	0930	11.38	0945	10.90	0.48
3 Jul 2005	2110	10.14	2100	9.90	0.24
10 Jun 2003	1010	8.21	1015	7.40	0.81
13 Jul 2004	0930	10.22	0930	9.90	0.32
28 Jul 2004	1025	9.05	1030	8.90	0.15
29 Jul 2004	0930	9.96	0930	9.40	0.56
25 Aug 2005	1015	10.18	1000	9.90	0.28
4 Sep 2005	0915	8.96	1000	8.90	0.06
				Average	0.34

4. Cloud-Top Height

The SEMEO technique for determining cloud-top height is described in Chapter 2, section C. Based on the assumptions that the SEMEO method requires, 30 cases were selected to test the SEMEO cloud-top height algorithm. One of the key SEMEO assumptions requires that the SST be representative of the surface air temperature. Because of this assumption, all 30 cases analyzed were tested using both the buoy SST and the air temperature measurements to identify which provided more accurate results. Additionally, the cloud-top brightness temperatures measured over the buoy, coincident in time with the measurements over Vandenberg, were compared to ensure similarity of the cloud top at both locations. This was required due to the approximate 20 miles separation between the buoy and the radiosonde launch site.

5. Modified Index of Refraction (M)

The SEMEO method of determining the refractive profile is described in Chapter 2, section D. Of the 30 cases that comprise Categories 1, 2, and 3, 14 were considered to be good candidates to test the refractive profile algorithm. Five of the cases came from Category 1, no cases from Category 2, and nine from Category 3. The reason for the other 17 cases being excluded from this test is based on possible errors in the dewpoint temperature profiles within the inversion, as discussed in Chapter 3, section B-1 and is illustrated in Fig. 16.

6. MODIS Water Vapor Analysis

There were 17 of the 30 cases that the water vapor images in MODIS were compared with their corresponding sounding profiles. This comparison was to determine if there were any indications in the water vapor images that correlated with the moisture gradient within the inversion layer. Three of the cases came from Category 1; two cases were from Category 2, and 12 cases from Category 3. The screening process to determine which soundings were used is described below.

First, the GOES channel 4 brightness temperatures were collected over Vandenberg at the time of the MODIS pass and at the time of the sounding. If the difference in brightness temperatures was one degree Celsius or less, then that case was set aside to compare with the MODIS channels. This procedure was done to ensure that the STBL over Vandenberg was well established and not changing much over the time difference between the MODIS pass and the sounding launch. Once the 17 cases were set aside, a *t*-test was conducted between the three categories using the brightness temperatures from the aforementioned seven MODIS channels to determine if the categories were statistically different. The *t*-test compared each channels average with the same channels average for each category. Additionally, the differences between channels were compared to the differences between the same channels for each category. The results indicated that there were no statistical difference between Categories 1 and 2; however, Category 3 was statistically different than Category 1 and Category 2. Based on the *t*-test results, Categories 1 and 2 cases were combined into one common category and compared with the 12 Category 3 cases.

IV. RESULTS

A. CLOUD TOP HEIGHTS RESULTS

1. Overview

The results of the SEMEO cloud-top height algorithm test for the selected 30 cases from Categories 1-3 are shown in Table 7. These cases were chosen based on the screening processes described in Chapter 3, section B-1. The cases are color-coded in the table: nine cases (black) are Category 1 soundings, seven cases (blue) are Category 2, and 14 cases (green) are from Category 3. Table 7 presents the results using SST as the input into the cloud-top height algorithm. Table 8 is structured and color-coded the same as Table 7 except that the buoy air temperature is used in the cloud height algorithm. The GOES Channel 4 brightness temperatures measured over the buoy are coincident in time with their associated Vandenberg soundings. The surface temperature used in the algorithm, SST (Table 7) or air temperature (Table 8), is the temperature measurement that the buoy recorded, also coincident in time with the Vandenberg sounding. The measured cloud-top height was selected by manual inspection of the Vandenberg sounding, which is used as verification for the SEMEO algorithm. The predicted cloud-top height was calculated from the SEMEO algorithm. One of the requirements within the cloud-top height algorithm is that the cloud-top brightness temperature is colder than the surface temperature. Because of this physical requirement, the SEMEO algorithm could not compute results for 3 of the 30 cases using SST, and 2 of the 30 cases using air temperature. For these cases in Tables 7 and 8, not available (N/A) is listed as the predicted height.

The RMS error for the 27 cases using SST for the surface temperature is 160.0m, and 148.9m for the 28 cases using the buoy air temperature. Standard deviation is 226.6m (SST) and 206.6m (air temperature). These results indicate that the air temperature measurements are more accurate for this dataset. This may be a result of the SST measurement, taken 0.6m below the surface, not responding as quickly as the air temperature measurement to changes in the surface temperature conditions. The average predicted cloud-top height is 532.4m (SST) and 556.0m (air temperature).

Table 7. Results from the cloud-top height algorithm, computed using the sea surface temperature, for 30 cases are color-coded by category: Category 1 (black), Category 2 (blue), and Category 3 (green). Input values for the algorithm are the GOES cloud-top brightness temperature (Ch.4, C) and buoy 46011 sea surface temperature (C). Measured cloud-top height (m) is from the Vandenberg AFB radiosonde. Predicted height (m) is the result of the cloud-top height algorithm. Height error (m) is computed and a negative error indicates the algorithm underestimates the height. Predicted height of N/A indicates the input values failed an algorithm requirement and no value was computed.

Date	Time (UTC)	GOES Ch. 4 (C)	SST (C)	Measured Cloud-top Height (m)	Predicted (SEMEO) Height (m)	Height Error (m)
28 Jun 2003	0000	12.9	14.2	266.2	177.4	-88.9
30 Jun 2003	0000	10.9	13.6	475.4	368.4	-107.0
10 Jul 2003	1200	10.4	10.3	237.7	N/A	-237.7
19 Aug 2003	0000	12.4	13.6	527.9	163.7	-364.2
31 Aug 2003	0000	11.4	13.6	460.4	300.2	-160.2
17 Sep 2004	0000	12.9	16.5	457.3	415.3	-42.0
25 Sep 2004	0000	11.9	14.9	319.8	409.3	89.5
5 Jul 2005	0000	10.9	13.4	513.6	341.1	-172.5
16 Sep 2005	1200	7.4	13.4	731.0	692.2	-38.8
23 May 2003	0000	9.4	10.5	388.2	150.1	-238.1
7 Jul 2003	0000	11.4	11.3	371.5	N/A	-371.5
11 Jul 2003	1200	10.9	10.2	166.3	N/A	-166.3
4 Jun 2005	0000	9.4	12.1	485.4	368.4	-117.0
4 Jul 2005	0000	9.9	13.3	505.6	463.9	-41.7
6 Jul 2005	0000	9.4	12.6	579.5	436.6	-142.9
4 Aug 2005	0000	12.9	15.3	277.2	327.5	50.2
10 Jun 2003	1200	7.4	14.9	1221.3	865.3	-356.0
12 Jun 2003	0000	6.4	15.2	1091.1	1015.3	-75.9
29 Jun 2003	1200	9.9	13.6	429.2	426.9	-2.4
6 Jul 2003	1200	8.9	11.7	385.0	382.0	-3.0
29 Apr 2004	1200	5.4	12.5	799.2	819.1	19.9
10 Jul 2004	1200	9.4	14.4	456.5	576.9	120.4
13 Jul 2004	1200	9.9	13.7	503.9	438.4	-65.5
28 Jul 2004	1200	8.9	15.2	623.1	726.8	103.7
29 Jul 2004	1200	9.4	15.7	639.3	726.8	87.5
2 Aug 2004	1200	7.4	13.7	922.1	726.8	-195.2
14 Aug 2005	0000	9.4	15.6	839.5	715.3	-124.2
25 Aug 2005	1200	9.9	14.9	354.8	576.9	222.0
4 Sep 2005	1200	8.9	15.6	451.2	773.0	321.8
13 May 2006	1200	7.4	11.4	493.2	461.5	-31.7

Table 8. Results from the cloud-top height algorithm, computed using the air temperature, for 30 cases are color-coded by category: Category 1 (black), Category 2 (blue), and Category 3 (green). Input values for the algorithm are the GOES cloud-top brightness temperature (Ch.4, C) and buoy 46011 air temperature (C). Measured cloud-top height (m) is from the Vandenberg AFB radiosonde. Predicted height (m) is the result of the cloud-top height algorithm. Height error (m) is computed and a negative error indicates the algorithm underestimates the height. Predicted height of N/A indicates the input values failed an algorithm requirement and no value was computed.

Date	Time (UTC)	GOES Ch. 4 (C)	Air Temp (C)	Measured Cloud-top Height (m)	Predicted (SEMEO) Height (m)	Height Error (m)
28 Jun 2003	0000	12.9	13.4	266.2	68.2	-198.0
30 Jun 2003	0000	10.9	13.7	475.4	382.0	-93.4
10 Jul 2003	1200	10.4	10.3	237.7	N/A	-237.7
19 Aug 2003	0000	12.4	15.0	527.9	354.7	-173.2
31 Aug 2003	0000	11.4	14.1	460.4	368.4	-92.0
17 Sep 2004	0000	12.9	15.9	457.3	409.3	-48.0
25 Sep 2004	0000	11.9	14.4	319.8	341.1	21.3
5 Jul 2005	0000	10.9	13.6	513.6	368.4	-145.2
16 Sep 2005	1200	7.4	13.7	731.0	726.8	-4.1
23 May 2003	0000	9.4	10.5	388.2	150.1	-238.1
7 Jul 2003	0000	11.4	12.6	371.5	163.7	-207.8
11 Jul 2003	1200	10.9	10.6	166.3	N/A	-166.3
4 Jun 2005	0000	9.4	12.1	485.4	368.4	-117.0
4 Jul 2005	0000	9.9	13.4	505.6	403.8	-101.8
6 Jul 2005	0000	9.4	13.3	579.5	449.9	-129.6
4 Aug 2005	0000	12.9	14.5	277.2	218.3	-58.9
10 Jun 2003	1200	7.4	14.0	1221.3	761.4	-459.8
12 Jun 2003	0000	6.4	13.5	1091.1	819.1	-272.0
29 Jun 2003	1200	9.9	12.6	429.2	368.4	-60.8
6 Jul 2003	1200	8.9	11.0	385.0	286.5	-98.5
29 Apr 2004	1200	5.4	12.1	799.2	773.0	-26.3
10 Jul 2004	1200	9.4	14.1	456.5	542.2	85.8
13 Jul 2004	1200	9.9	13.3	503.9	463.9	-40.0
28 Jul 2004	1200	8.9	14.4	623.1	634.5	11.4
29 Jul 2004	1200	9.4	15.0	639.3	646.1	6.7
2 Aug 2004	1200	7.4	14.9	922.1	865.3	-56.8
14 Aug 2005	0000	9.4	14.8	839.5	623.0	-216.5
25 Aug 2005	1200	9.9	12.9	354.8	409.3	54.5
4 Sep 2005	1200	8.9	12.8	451.2	449.9	-1.2
13 May 2006	1200	7.4	11.1	493.2	426.9	-66.3

2. Distinguishing Features Between the Cases

As seen in Tables 7 and 8, there are some cases that the SEMEO algorithm predicted very well, and others that were not estimated well. There are several reasons that account for the varying degrees of success and will be discussed below. In analyzing the cases that had the best results, the following features were most common.

Figure 17 illustrates three features that are common when analyzing the soundings profiles and their associated relative humidity profiles. The temperature and dewpoint temperature profiles clearly indicate that the sounding was in cloud. This is evident when the two profiles either merge or come within a degree from one another and often remain together for several hundred meters. This is also supported in the relative humidity graph which indicates greater than 95% relative humidity when the two profiles are together. Additionally, when analyzing the soundings that have the best results, the depth of the cloud layer is several hundred meters and the associated inversion at the cloud top is generally above 400 meters.

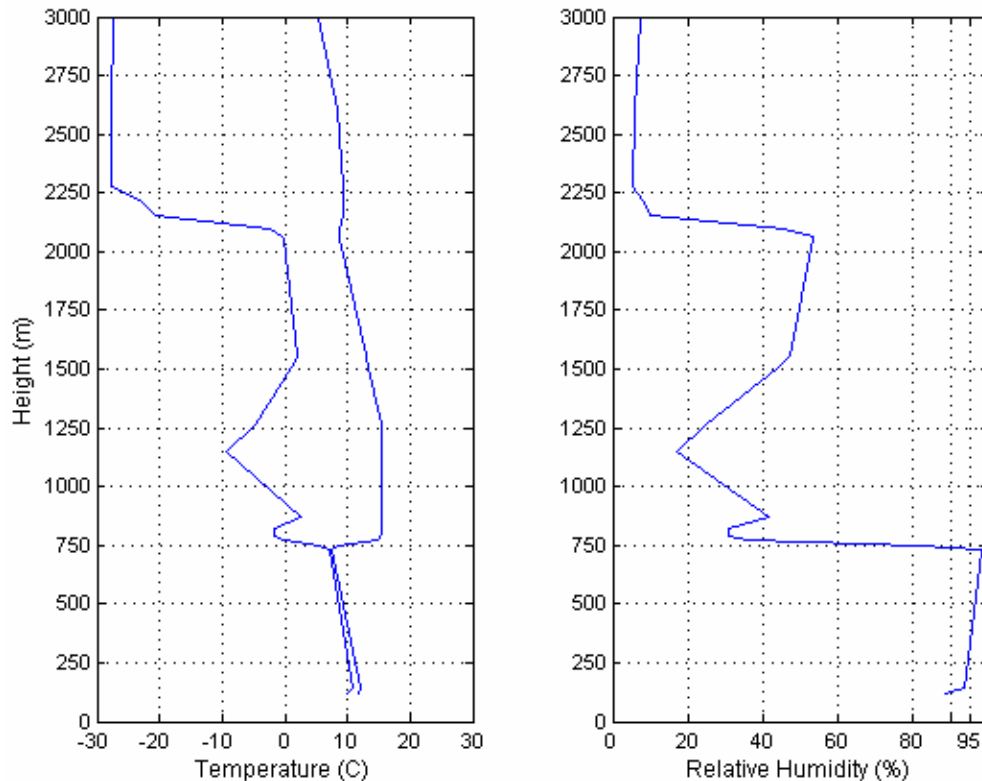


Fig. 17. The cloud-top height algorithm typically has success with profiles similar to this Vandenberg sounding at 1200 UTC 16 September 2005. The sounding has a deep cloud layer and a well-defined inversion.

Another common feature is evident in the associated 500mb height field. The cases with the most success were generally under the influence of a troughing feature aloft, as evident in the 500mb heights charts. This troughing feature is observed in 11 of 15 cases in Table 8 that have an estimated height error of less than 100m. This feature is seen in Fig. 18, where the 500mb heights are superimposed on the GOES-10 infrared image.

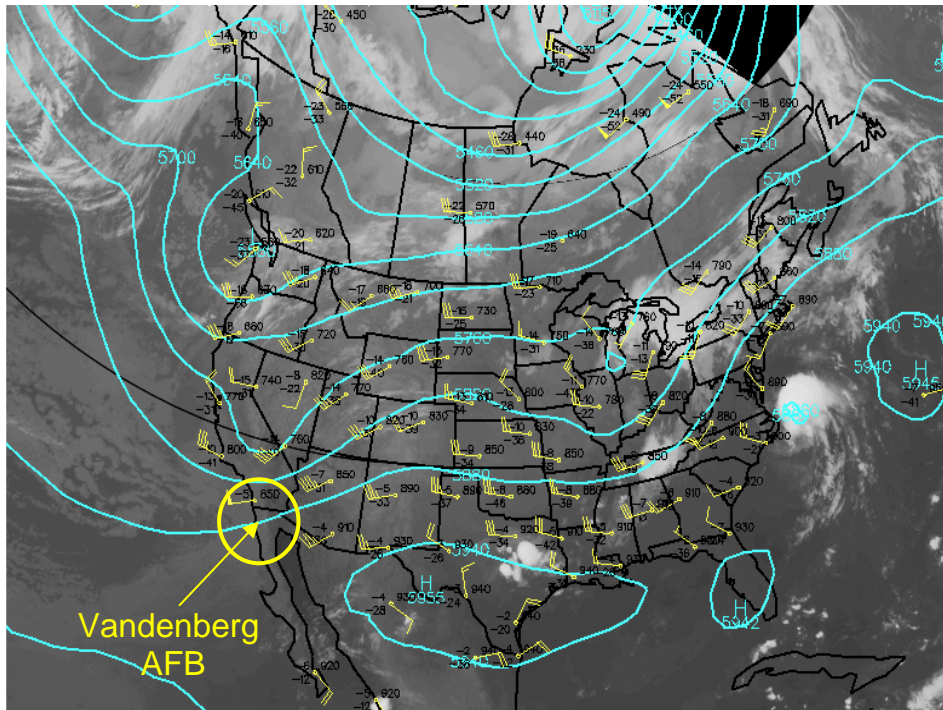


Fig. 18. 500mb heights are superimposed on the GOES-10 infrared image for 1200 UTC 16 September 2005. The 500mb trough over Vandenberg AFB is observed in 11 of 15 cases in Table 8 that have an estimated height error of less than 100m (Image from San Francisco State University 2006).

The next common feature among the successful cases supports the assumption that the boundary layer must be well mixed. This is apparent from plots of potential temperature for each case. The potential temperature line is vertical when the layer is well mixed. Figure 19 illustrates the potential temperature and specific humidity profiles for the 16 September 2005 case. Shown in Fig. 19 is a near vertical line up to 731 meters. At this point the potential temperature increases rapidly as the sounding enters the inversion layer and exits the well-mixed region below. Sounding data points (i.e.,

mandatory and significant reporting levels) are indicated by the red crosses on the blue lines in Fig. 19.

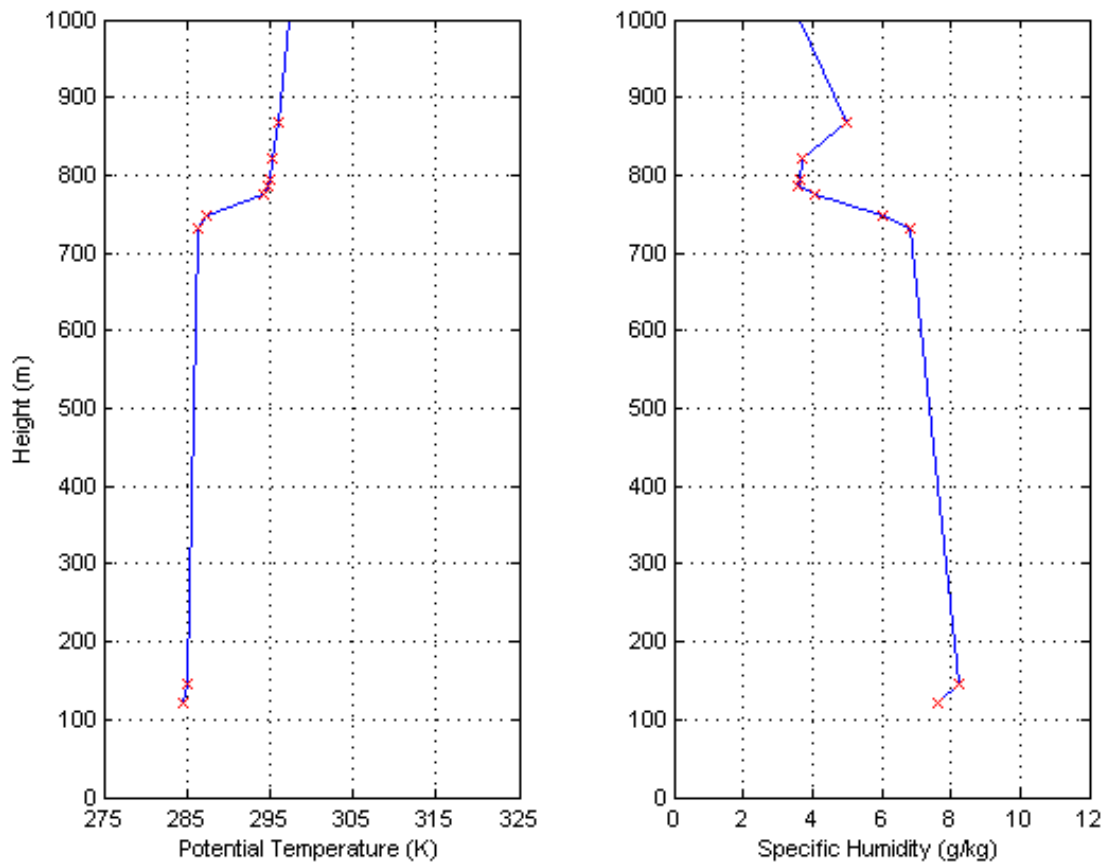


Fig. 19. Potential temperature and specific humidity graph for 1200 UTC 16 September 2005. The near vertical potential temperature line illustrates the well-mixed boundary layer. The red crosses represent the sounding data points from mandatory and significant reporting levels.

Another common feature is found when comparing soundings launched during the day versus soundings launched at the night, as seen in Fig. 20. There are 14 (of 27) SST cases that occurred at 1700 LT (day) and 13 that occurred at 0500 LT (night). The RMS error for the day cases is 154.3m, and 165.9m for the night cases. Although the RMS error for the day cases is lower, a better comparison is an analysis of the fractional percentage errors between the day and night cases. For the day cases the average cloud-top height is 403.7m, yielding a fractional percentage error of 38%. For the night cases, the average cloud-top height is 630.2m, yielding a fractional error estimation of 26%.

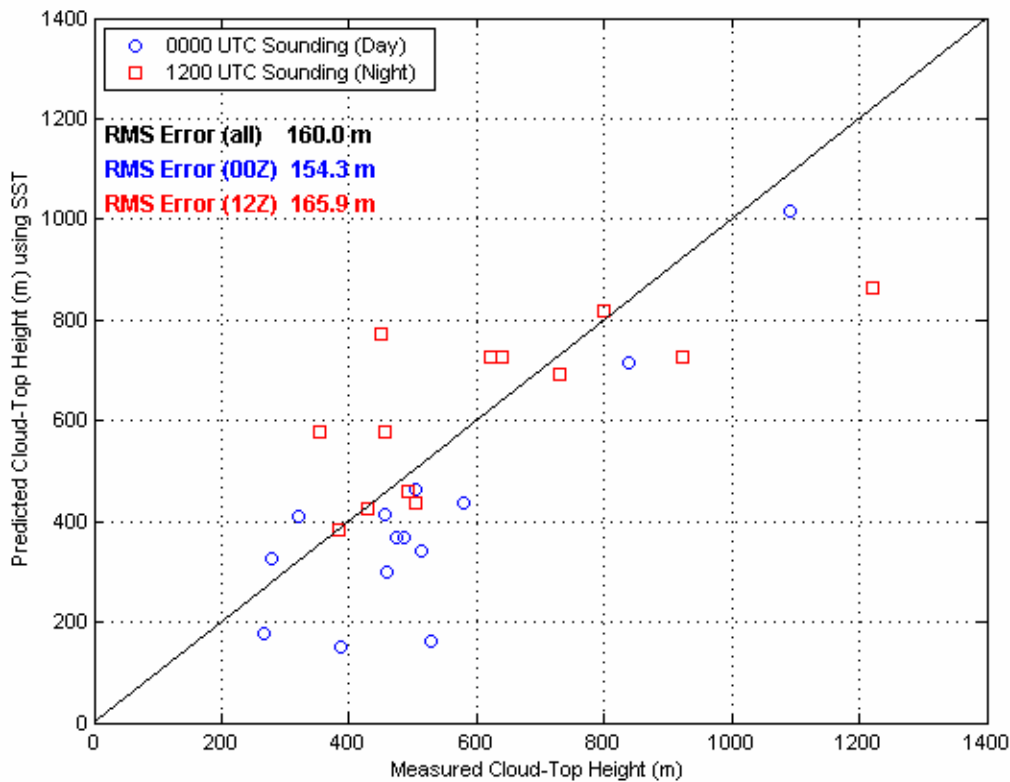


Fig. 20. Scatterplot of measured cloud-top height (m) versus SEMEO predicted height (m) using SST as the input surface temperature. The black line is the one-to-one line, which indicates no error. The day cases (blue) and night cases (red) are indicated. The RMS error (m) of all 27 cases, 14 day, and 13 night cases is listed

Analysis of the 28 cases using air temperature indicate a slight improvement for the day cases and a significant improvement for the night cases (compared to SST input), as seen Fig. 21. There are 15 day cases (1700 LT) and 13 night cases (0500 LT). The RMS error for the day cases is 158.2m, and is 137.4m for the night cases. For the day cases, the average cloud-top height is 503.9m, yielding a fractional percentage error of 31%. For the night cases, the average cloud-top height is 616m, yielding a fractional error of 22%. The air temperature results for the night cases indicate an improvement in both RMS error and fractional percentage error when compared to SST results. These improvements indicate that the surface temperature is better represented at 0500 LT with the air temperature measurement as algorithm input.

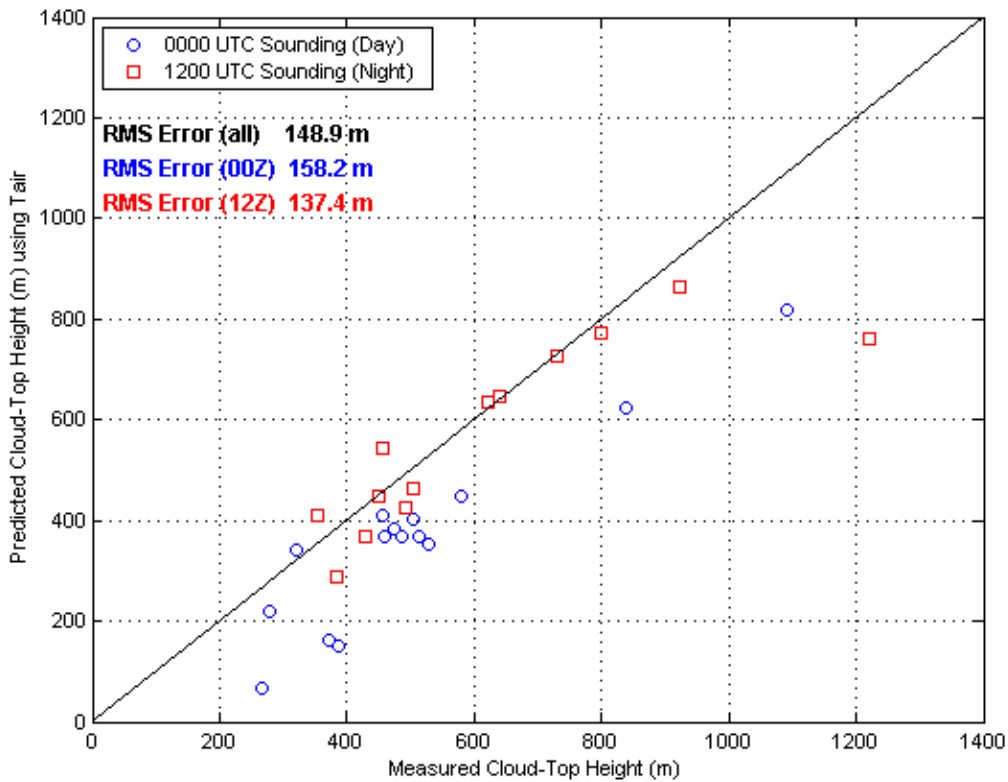


Fig. 21. Scatterplot of measured cloud-top height (m) versus SEMEO predicted height (m) using air temperature as the input surface temperature. The black line is the one-to-one line, which indicates no error. The day cases (blue) and night cases (red) are indicated. The RMS error (m) of all 28 cases, 15 day, and 13 night cases is listed.

The final commonality between the more successful cases is seen in Fig. 22, where cases with a temperature difference of more than three degrees Celsius between Channel 4 brightness temperature and surface temperature (using SST), are compared to those with less than or equal to a three degrees Celsius difference. The accuracy of the cloud-top height algorithm generally improves as this difference increases. There are 17 of the 27 SST cases that indicate a difference greater than three degrees. The RMS error for the 17 cases is 154m and for the remaining 10 cases is 169.8m. The average cloud-top height estimate for the 17 cases is 637.9m, yielding a fractional percentage error of 24%. The average cloud-top height estimate for the remaining 10 cases is 412.7m with a fractional percentage error of 41%.

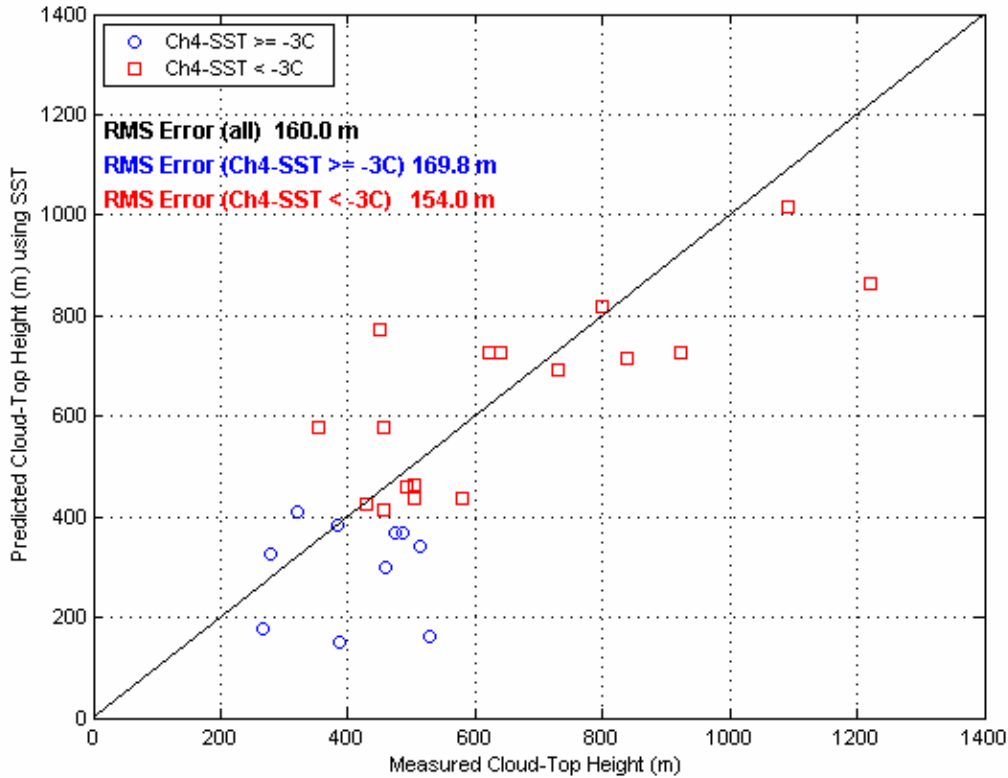


Fig. 22. Scatterplot of measured cloud-top height (m) versus SEMEO predicted height (m) using SST as the input surface temperature. The black line is the one-to-one line, which indicates no error. Cases are separated based on brightness temperature and surface temperature difference. Shallow STBL cases (Ch4-SST \geq -3C) are denoted in blue, and deeper STBL cases (Ch4-SST $<$ -3C) are denoted in red. The RMS error (m) of all 27 cases, 10 shallow, and 17 deep cases is listed

Similarly to Fig. 22, Fig. 23 separates the SEMEO cloud-top height results using air temperature based on brightness temperature and surface temperature difference. There are 14 with a temperature difference of greater than or equal to -3C and 14 cases less than -3C. The RMS error is 131.9m and 164.1m, respectively. The average cloud-top height estimate for the 14 cases with greater than three degrees difference is 704m and 408m for the remaining 14 cases. The fractional percentage error is 23% and 32%, respectively. The difference here between the air temperature results and SST results should not be compared because the datasets are not at similar. There are 14 cases in each group for the air temperature, and for the SST cases the split is 17 and 10.

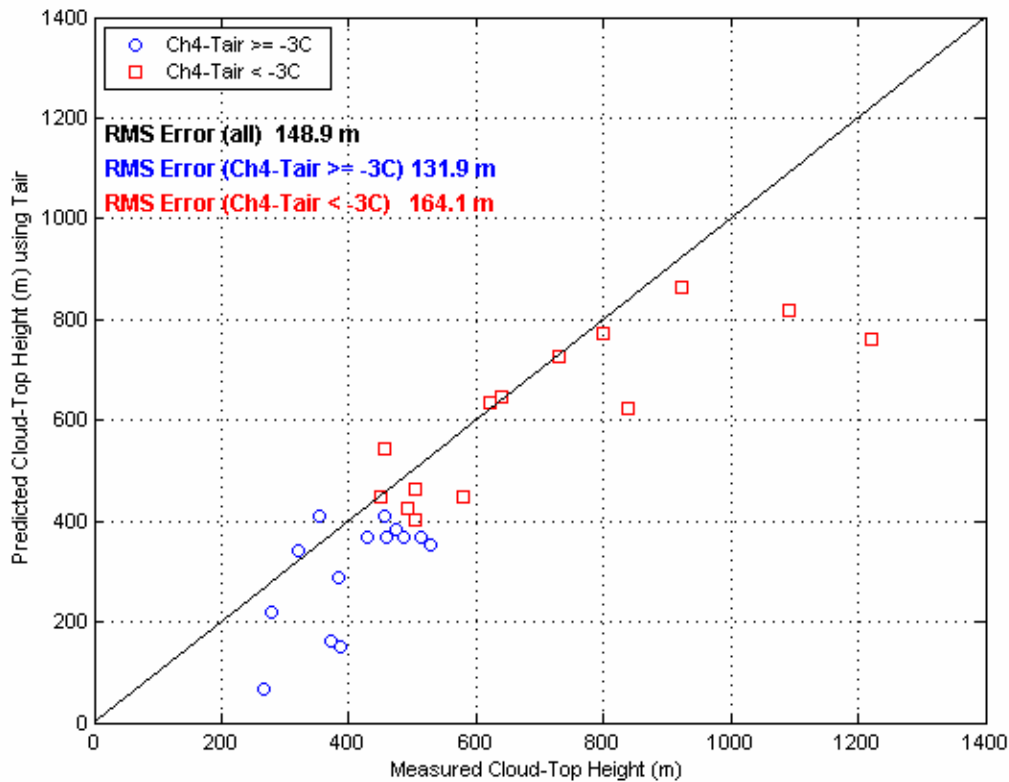


Fig. 23. Scatterplot of measured cloud-top height (m) versus SEMEO predicted height (m) using air temperature as input. The black line is the one-to-one line, which indicates no error. Cases are separated based on brightness temperature and surface temperature difference. Shallow STBL cases (Ch4-Tair \geq -3C) are denoted in blue, and deeper STBL cases (Ch4-Tair $<$ -3C) are denoted in red. The RMS error (m) of all 28 cases, 14 shallow, and 14 deep cases is listed.

3. Case Examples

Figure 24 shows the 0000 UTC sounding for 12 June 2003 and illustrates the previous discussion for the more successful cases, with the exception that this sounding was not launched during the local night time. This sounding does indicate a very deep cloud layer (~700meters) with the associated inversion occurring at 1091.1 meters. The estimated cloud top height is 1015.3 meters yielding an underestimation of 75.9 meters. The fractional percentage error is within 7%. The red stars superimposed on the red line in Fig. 24 depict the three points generated by the cloud-top height algorithm. The first point is the input surface temperature (SST) and the starting location for the estimated profile. The second point in the middle represents the estimated cloud base. The third point at the top indicates the estimated cloud-top height.

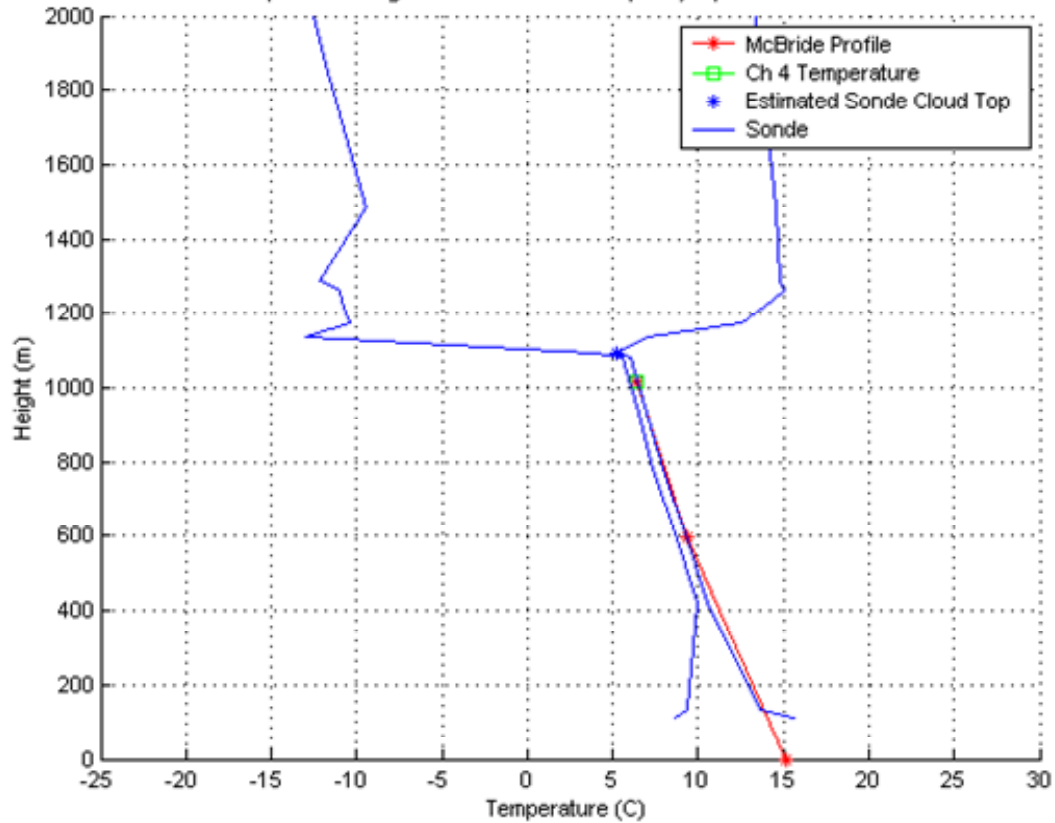


Fig. 24. Vandenberg sounding for 0000 UTC 12 June 2003. The blue lines indicate the temperature and dewpoint temperature profiles. The red line with three red stars superimposed indicates the three points generated from the cloud-top height algorithm (surface, cloud base, and cloud top).

The GOES-10 brightness temperature is 6.2 degrees Celsius and the SST is 15.2 degrees Celsius. The difference between these two measurements is 8.8 degrees Celsius. This supports the observation that the more successful cases have temperature differences greater than three degrees Celsius. The 500mb analysis heights chart is shown in Fig. 25 and indicates an approaching trough. The approaching trough provides the upper-level dynamics that support the deep boundary layer by reducing the subsidence aloft.

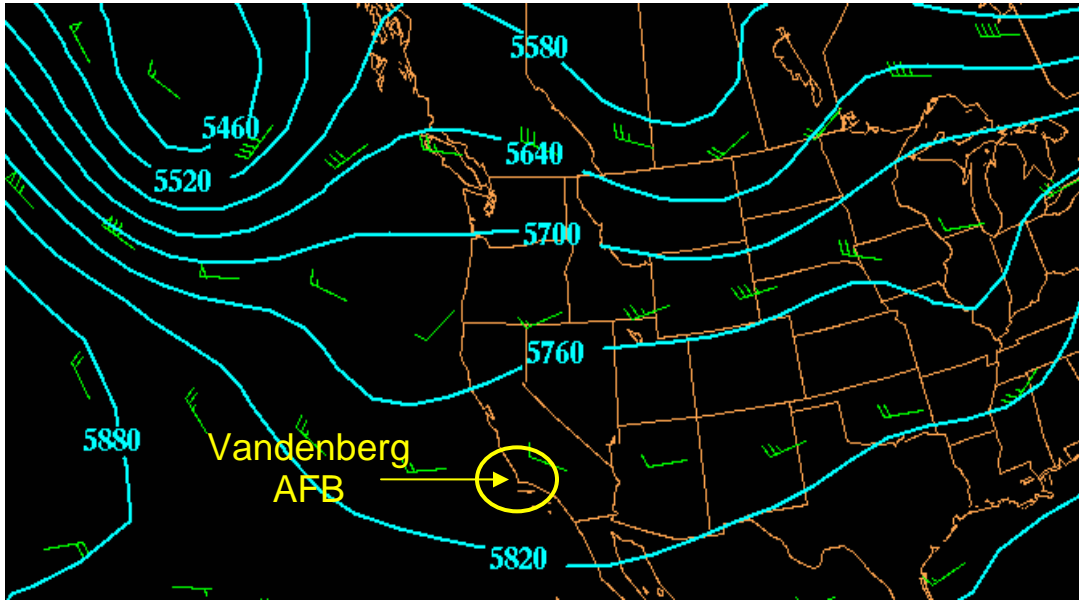


Fig. 25. 500mb height analysis for 0000 UTC 12 June 2003 indicating a trough approaching Vandenberg AFB from the West.

The case just described, 12 June 2003, has the second highest cloud-top height of the 30 cases. The only case with a higher cloud-top height is 10 June 2003, and its cloud-top height is underestimated by 459.8 meters. Through analysis of the potential temperature profile for the 10 June 2003 case, it appears that the boundary layer may have been decoupled and therefore is not well mixed. This violates the well-mixed assumption of the SEMEO technique and provides reasoning for the 459.8m error.

The next example case is from 0000 UTC 28 June 2003 and represents what is commonly found in cases that were poorly estimated. Figure 26 presents the temperature and dewpoint temperature profiles as well as the corresponding relative humidity values. Figure 26 indicates a shallow cloud layer and corresponding lower than average cloud-top height. The relative humidity graph indicates an approximately 100m layer where the relative humidity was greater than 95%. This is probably an overestimation because the dewpoint temperature profile is not drying out immediately above the cloud top. The measured cloud-top height for this case is 266.2 meters and the predicted height is 177.4 meters. This is an underestimation of 88.9 meters and a fractional percentage error of 33%. Additionally, the GOES-10 brightness temperature is 12.9 degrees Celsius and the SST is 14.2 degrees Celsius. The difference between these two measurements is 1.3

degrees Celsius, which is much less than the average of 3.84 degrees Celsius for all 30 cases. When the difference between cloud-top brightness temperature and surface temperature is small, the likelihood of the case being underestimated is higher. This was illustrated previously in Figs. 22-23.

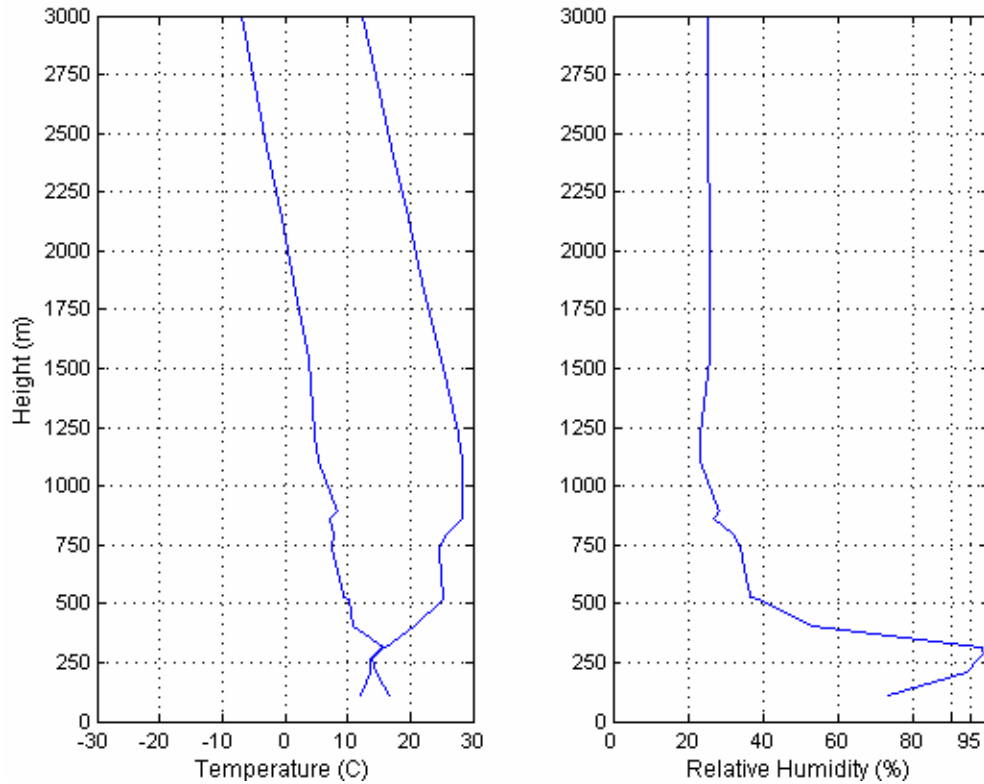


Fig. 26. Vandenberg AFB sounding for 0000 UTC 28 June 2003. The dewpoint temperature increase above the top of the STBL (266.2m) is assumed to be erroneous.

The 500mb height analysis is shown in Fig. 27, and indicates high pressure over Vandenberg AFB. The result of the high pressure is increased subsidence on top of the inversion. This is also a common feature among the cases with large errors in their cloud-top height estimates.

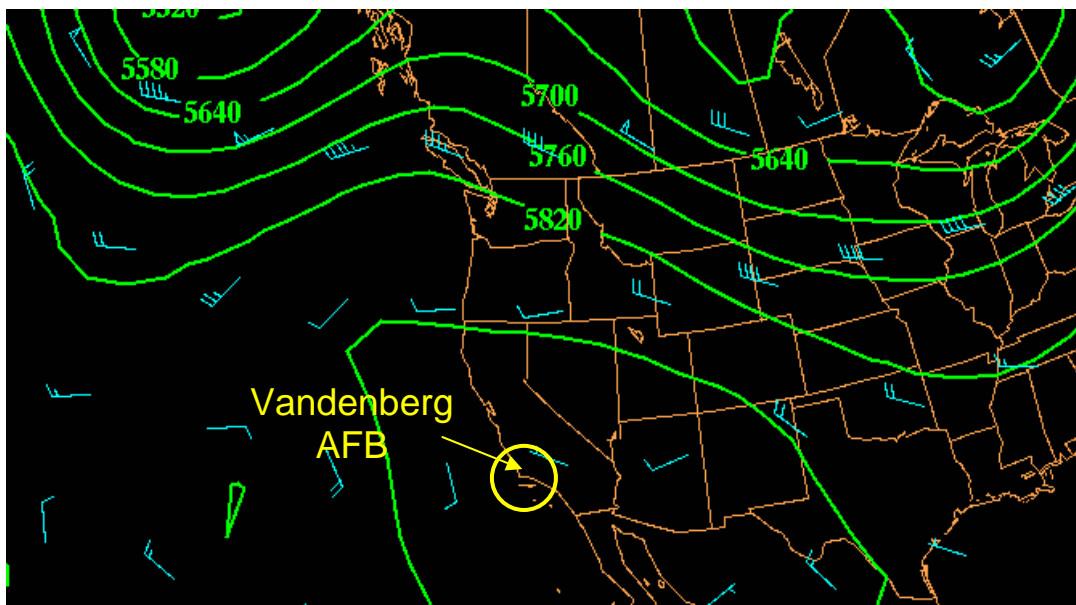


Fig. 27. 500mb height analysis for 0000 UTC 28 June 2003 indicating a high pressure region above Vandenberg. AFB.

B. MODIFIED INDEX OF REFRACTION (M) RESULTS

1. Modifications to Radiosonde Profiles

Fourteen out of the 30 final cases were analyzed with the refractive part of the SEMEO program. For the soundings in which the dewpoint temperature increased above the inversion, errors due to wetting of the sensor were assumed, and those data points were identified and removed from the profile. The 14 cases used here have three or less dewpoint temperature values removed. Discussion of why this occurs was described in Chapter 3 section B-1. Figures 28 and 29 are examples of how the profiles changed once the bad data-points were removed. The dashed blue line indicates the original sounding profile within the inversion. The red line indicates the modified profile. This new profile was created by connecting the first dewpoint temperature measurement that was less than the dewpoint temperature measured at the temperature inversion together via a straight line. It is unknown if this exactly replicates reality, however, it is assumed that it is closer than the reported sounding.

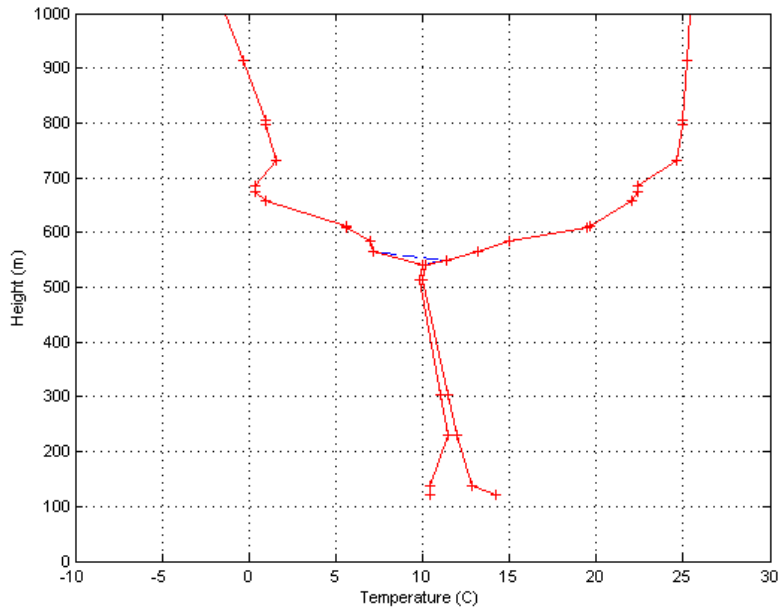


Fig. 28. Modified dewpoint temperature profile for 0000 UTC 5 July 2005. Modifications to the original profile were made to remove dewpoint temperature data points that indicated increased dewpoint values above the cloud top. The blue dashed line represents the original dewpoint temperature profile; the red line is the modified profile.

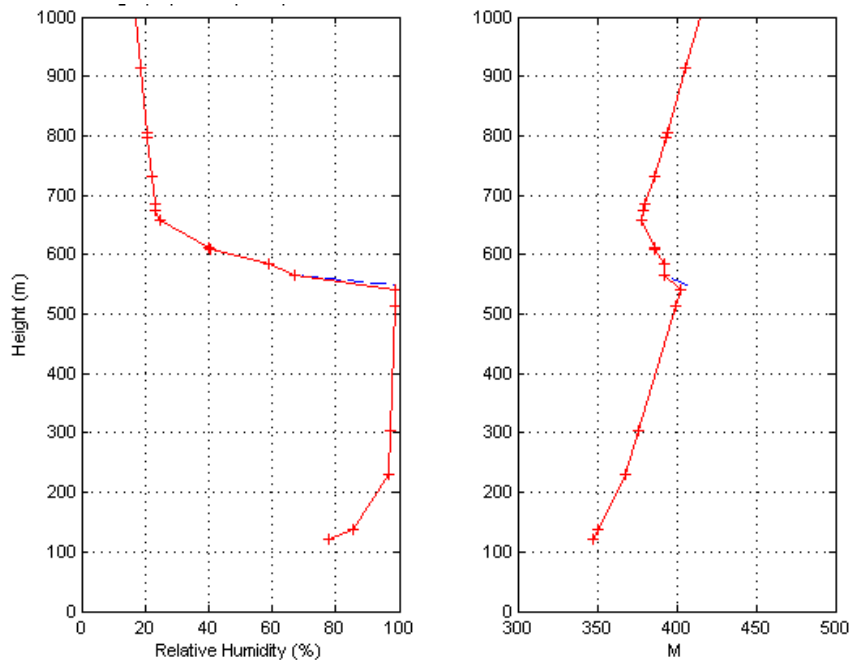


Fig. 29. Modified RH and M profiles for 0000 UTC 5 July 2005. Modifications to the original profiles were made to remove bad data points that resulted from errors in the dewpoint temperature profile. The blue dashed line represents the original relative humidity and M profiles and the red lines are the modified profiles.

2. Modified Index of Refraction Results for Category 1

Table 9 lists the SEMEO results for Category 1 using SST as input for the surface temperature. The strength of the trapping layer (ΔM , or M-strength) calculated by the radiosonde and the SEMEO program are seen in columns three and four respectively. The ΔM error column indicates the results after subtracting the measured values from the predicted. A positive number indicates that the SEMEO program overestimated the M-strength. The trapping layer depth error column is set up similarly, where a positive error result indicates an overestimation by the SEMEO program. The trapping layer depth error is calculated by subtracting the measured depth from the predicted depth, which is fixed (100m). For Category 1, all five cases indicate that the SEMEO program overestimated the M-strength. The average predicted ΔM is 41.3 with an associated RMS error of 24.2, and a standard deviation of 7.0. Additionally, the trapping layer depth assumption of 100m is an overestimation four out of five times for Category 1 by the SEMEO program.

Overestimating the results of both M-strength and layer thickness can give the user an inaccurate understanding of the refractive environment. Overestimations can result in predicting surface-based ducts that are not present. Additionally, if the duct thickness is overestimated, a user may erroneously believe that some frequencies will be trapped.

Table 9. Trapping layer statistics for Category 1 cases using SST as the surface temperature input for the SEMEO algorithm. Radiosonde measurements of trapping layer strength (ΔM , unitless) and depth (m) are compared with the SEMEO predictions of strength and depth. Positive errors indicate the SEMEO algorithm overestimated layer strength or depth. The SEMEO algorithm uses a 100m trapping layer depth for all cases.

Date	Time (UTC)	Measured ΔM	Predicted ΔM using SST	ΔM Error	Measured Trapping Layer Depth (m)	Predicted Trapping Layer Depth (m)	Trapping Layer Depth Error (m)
30 Jun 2003	0000	23.21	44.02	20.81	125.0	100.0	-25.0
19 Aug 2003	0000	9.13	47.29	38.16	89.1	100.0	10.9
25 Sep 2004	0000	25.01	42.29	17.28	61.4	100.0	38.7
5 Jul 2005	0000	16.78	43.62	26.84	71.3	100.0	28.7
16 Sep 2005	1200	24.32	29.24	4.92	53.9	100.0	46.1

All columns in Table 10 are the same as Table 9, with the exception of column three, “Predicted ΔM using Tair”. This column indicates that the surface temperatures used in the SEMEO program were from the air temperature measurements at the buoy instead of the SST measurements. The results using air temperature are similar to the above SST results, indicating that SEMEO overestimates the M-strength for all five cases. The average predicted ΔM calculated by SEMEO is 40.8, with an RMS error of 23.6 and a standard deviation of 6.8. The fixed 100m trapping layer depth within the SEMEO program overestimates the trapping layer four out of five times.

Table 10. Trapping layer statistics for Category 1 cases using air temperature as the surface temperature input for the SEMEO algorithm. Radiosonde measurements of trapping layer strength (ΔM , unitless) and depth (m) are compared with the SEMEO predictions of strength and depth. Positive errors indicate the SEMEO algorithm overestimated layer strength or depth. The SEMEO algorithm uses a 100m trapping layer depth for all cases.

Date	Time (UTC)	Measured ΔM	Predicted ΔM using Tair	ΔM Error	Measured Trapping Layer Depth (m)	Predicted Trapping Layer Depth (m)	Trapping Layer Depth Error (m)
30 Jun 2003	0000	23.21	43.87	20.66	125.0	100.0	-25.0
19 Aug 2003	0000	9.13	45.12	35.99	89.1	100.0	10.9
25 Sep 2004	0000	25.01	43.06	18.05	61.4	100.0	38.7
5 Jul 2005	0000	16.78	43.31	26.53	71.3	100.0	28.7
16 Sep 2005	1200	24.32	28.84	4.52	53.9	100.0	46.1

3. Modified Index of Refraction Results for Category 2

No cases from Category 2 are compared to the refractive profiles from the SEMEO program. This was due to the excessive amount (more than three) of bad data points required to be removed from the radiosonde's dewpoint temperature profiles within the trapping layer. When more than three points were removed, the resulting radiosonde dewpoint temperature profile could not be assumed to be accurately represented.

4. Modified Index of Refraction Results for Category 3

Table 11 illustrates the SEMEO results for Category 3 using SST input for the representative surface temperature. For Category 3, there are seven cases where the M-strength is overestimated and two cases that are underestimated. The average predicted ΔM is 35.9. The corresponding RMS error is 5.8 with a standard deviation of 7.2. The average measured trapping layer thickness for the radiosondes is 66 meters with a standard deviation of 20m. The average thickness for the SEMEO program remains fixed at 100 meters. Eight out of nine cases are overestimated by the SEMEO assumption of

100m. As mentioned above, overestimating the trapping layer thickness can lead a user to conclusions about the refractive environment that are not accurate.

Table 11. Trapping layer statistics for Category 3 cases using SST as the surface temperature input for the SEMEO algorithm. Radiosonde measurements of trapping layer strength (ΔM , unitless) and depth (m) are compared with the SEMEO predictions of strength and depth. Positive errors indicate the SEMEO algorithm overestimated layer strength or depth. The SEMEO algorithm uses a 100m trapping layer depth for all cases.

Date	Time (UTC)	Measured ΔM	Predicted ΔM using SST	ΔM Error	Measured Trapping Layer Depth (m)	Predicted Trapping Layer Depth (m)	Trapping Layer Depth Error (m)
10 Jun 2003	1200	30.81	26.72	-4.09	46.9	100.0	53.1
12 Jun 2003	0000	26.72	26.91	0.19	55.3	100.0	44.8
29 Jun 2003	1200	37.89	43.26	5.37	86.0	100.0	14.0
6 Jul 2003	1200	32.94	42.70	9.76	104.2	100.0	-4.2
29 Apr 2004	1200	19.11	26.15	7.04	63.0	100.0	37.0
13 Jul 2004	1200	30.43	40.05	9.62	61.6	100.0	38.4
28 Jul 2004	1200	36.71	39.45	2.74	79.9	100.0	20.1
29 Jul 2004	1200	36.85	39.91	3.06	62.3	100.0	37.7
14 Aug 2005	0000	38.16	37.51	-0.65	36.4	100.0	63.6

All columns in Table 12 are the same as Table 11 with the exception of column three, “predicted ΔM using T_{air} ”. This column indicates that the surface temperatures used in the SEMEO program are from the air temperature measurements at the buoy instead of SST measurements. For Category 3 using T_{air} , there are eight out of nine cases where the M-strength is overestimated and one that is underestimated. The average predicted ΔM is 36.8. The corresponding RMS error is 6.2 with a standard deviation of 6.9. The average measured trapping layer depth remains at 66 meters for the radiosonde with a standard deviation of 20m. The measured radiosonde results are independent and separate from the SEMEO program results.

Table 12. Trapping layer statistics for Category 3 cases using air temperature as the surface temperature input for the SEMEO algorithm. Radiosonde measurements of trapping layer strength (ΔM , unitless) and depth (m) are compared with the SEMEO predictions of strength and depth. Positive errors indicate the SEMEO algorithm overestimated layer strength or depth. The SEMEO algorithm uses a 100m trapping layer depth for all cases.

Date	Time (UTC)	Measured ΔM	Predicted ΔM using Tair	ΔM Error	Measured Trapping Layer Depth (m)	Predicted Trapping Layer Depth (m)	Trapping Layer Depth Error (m)
10 Jun 2003	1200	30.81	27.90	-2.91	46.9	100.0	53.1
12 Jun 2003	0000	26.72	29.14	2.42	55.3	100.0	44.8
29 Jun 2003	1200	37.89	43.93	6.04	86.0	100.0	14.0
6 Jul 2003	1200	32.94	43.79	10.85	104.2	100.0	-4.2
29 Apr 2004	1200	19.11	26.67	7.56	63.0	100.0	37.0
13 Jul 2004	1200	30.43	39.76	9.33	61.6	100.0	38.4
28 Jul 2004	1200	36.71	40.50	3.79	79.9	100.0	20.1
29 Jul 2004	1200	36.85	40.83	3.98	62.3	100.0	37.7
14 Aug 2005	0000	38.16	38.56	0.40	36.4	100.0	63.6

5. Examples of SEMEO's Refractive Results

Figure 30 illustrates the M-profile and sounding profile for 25 September 2004. The four red stars annotated on the radiosonde profile (right side) represent the height and temperature for the surface, LCL, cloud-top, and 850mb. The M profiles (left side) are from the sounding (blue) and the SEMEO predicted profile (red) using Tair as input. The five red stars on the red line represent the five points generated by the SEMEO program as described in Chapter 2, section D. For this case, the difference in M-units within the trapping layer predicted by SEMEO is 43.06. The measured radiosonde M difference is 36.71, resulting in an overestimation of 6.36. The trapping layer thickness is overestimated by 20.1 meters.

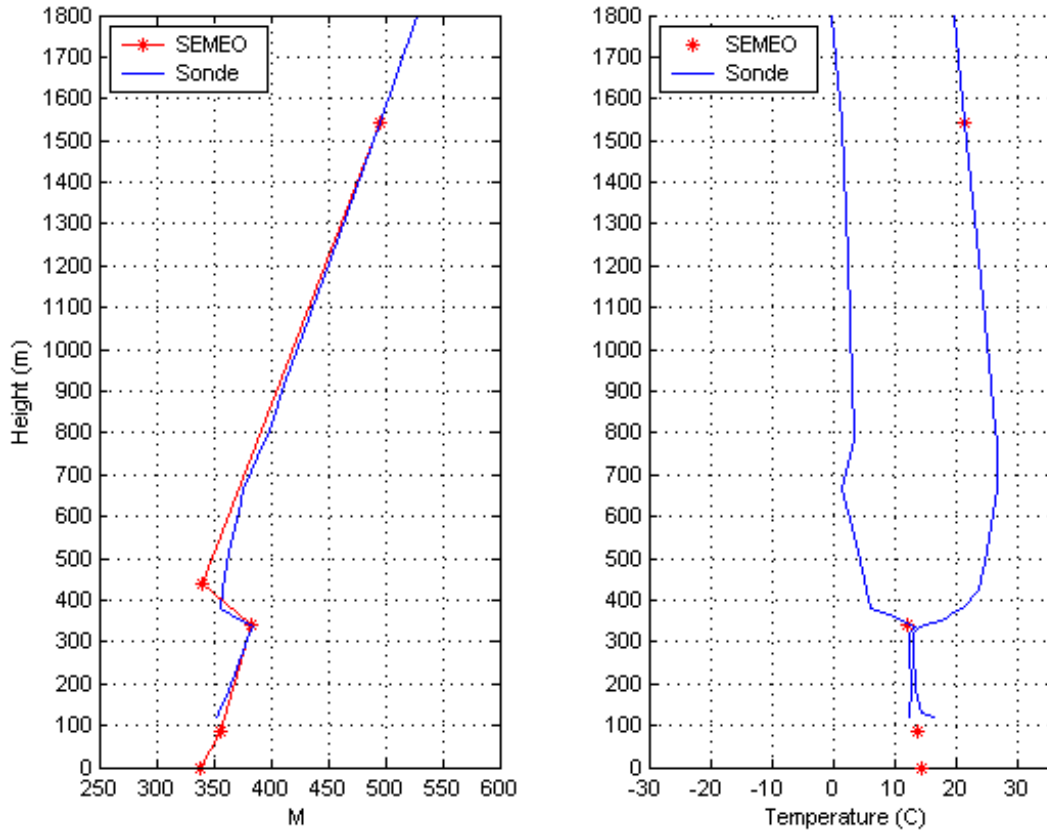


Fig. 30. SEMEO generated profile superimposed on the 0000 UTC 25 September 2004 Vandenberg AFB sounding. The five red stars on the left indicate the SEMEO generated points that are connected to create the predicted M profile. The red stars on the sounding graph on the right indicate the surface, cloud base, cloud top, and 850mb height and temperature.

Figure 31 depicts the 12 June 2003 results using SST as input into the SEMEO program. For this example, the difference in M-units within the trapping layer predicted by SEMEO is 25.86, while the measured radiosonde indicates the difference to be 26.72. These results indicate a slight underestimation of 0.86 M-units. The trapping layer thickness determined from the radiosonde is 55.25 meters, which indicates an overestimation of the trapping layer thickness by SEMEO of 44.75 meters.

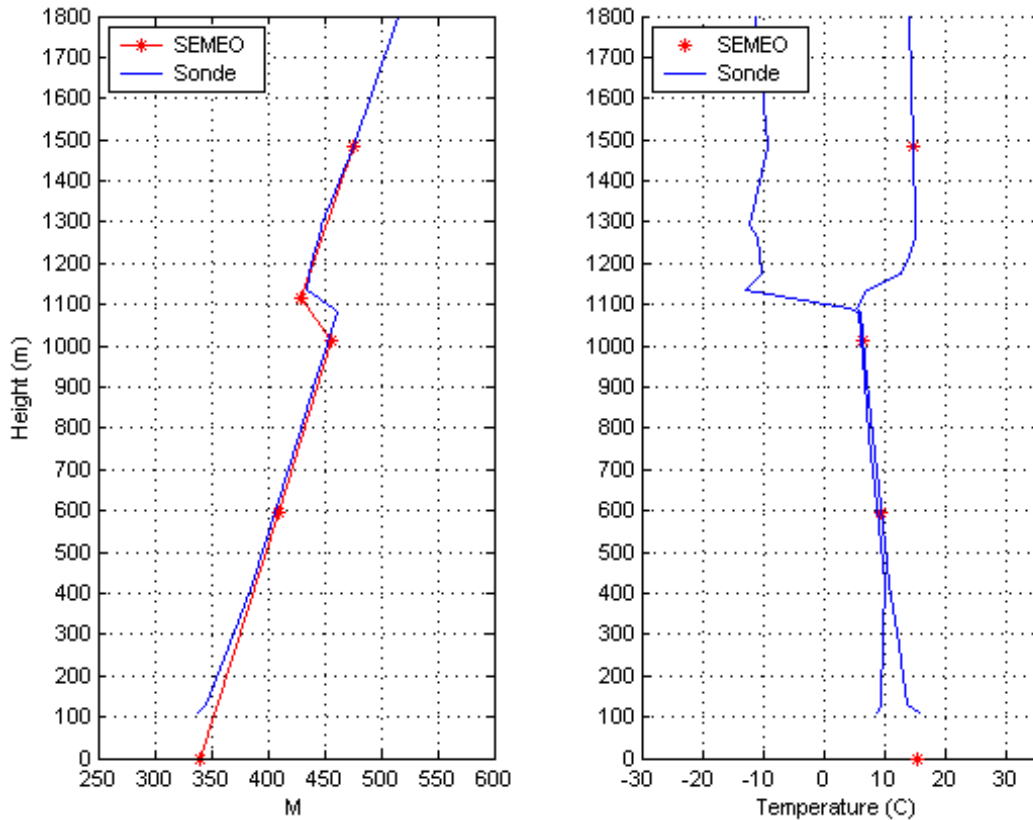


Fig. 31. SEMEO generated profile superimposed on the 1200 UTC 12 June 2003 Vandenberg AFB sounding. The five red stars on the left indicate the SEMEO generated points that are connected to create the predicted M profile. The red stars on the sounding graph on the right indicate the surface, cloud base, clout top, and 850mb height temperature.

6. Comparison Between Category 1 and Category 3

Figure 32 illustrates the difference in M-strength accuracy predicted by SEMEO for Categories 1 and 3 with SST input. Nearly all Category 3 cases show a better comparison with measured ΔM than Category 1 cases. When analyzing the measured M-strength generated by the modified radiosondes, Category 1 is overestimated on average by $\sim 100\%$. This error may be related to the $\Delta T'$ values generated with Eq. (13) and inputted into Eq. (14), yielding larger ΔM results. The $\Delta T'$ average is $\sim 20\%$ higher for Category 1 cases than for Category 3. Additionally the measured ΔM results from Category 3 are $\sim 33\%$ higher than Category 1, which is seen in Fig. 32.

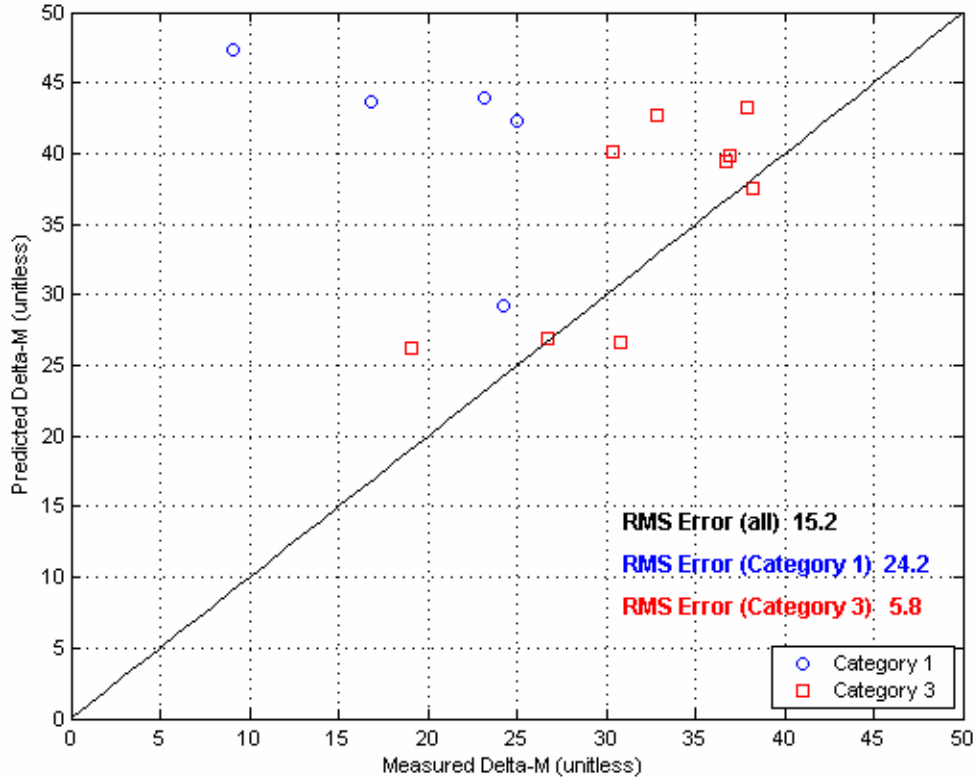


Fig.32 Scatterplot of predicted M-strength values for Category 1 versus Category 3. The black line is the one-to-one line, which indicates no error .

C. WATER VAPOR ANALYSIS RESULTS

The water vapor channels and images were analyzed to see if there is a signature within the water vapor pattern that can be correlated with the moisture gradient profile within the trapping layer. Tables 13 and 14 list the brightness temperatures measured over Vandenberg by the most time coincident MODIS pass available. As discussed in Chapter 3 section B-6, Categories 1 and 2 were combined based on their statistical similarities.

The average brightness temperature results for Category 3 indicate cooler temperatures for all channels measured when compared to the Category 1/2 combination. Channels 27 and 28 indicated the largest difference between the two categories. The brightness temperature results, and differencing between all channels within each category, did not indicate any correlating pattern that could be linked to the resulting moisture gradient within the inversion layer. The MODIS images from channels 20, 23, 27, 28, 29, 31, and 32 for the 17 cases found in Tables 13 and 14 were analyzed and

compared to their associated soundings. There were no definitive characteristics observed from the raw images or from image enhancements that could be correlated with the moisture gradient within the trapping layer. Image differencing techniques and enhancements of those images were also conducted with no definitive results.

Table 13. MODIS brightness temperatures (C) over Vandenberg AFB for Category 1 and 2 radiosondes. Channels 27-32. are affected by water vapor absorption.

Date	UTC	Ch. 27	Ch. 28	Ch. 29	Ch. 31	Ch. 32
10 Jul 2003	1025	-18.50	-5.49	8.58	9.68	10.32
16 Sep 2004	2115	-18.46	-3.15	12.66	14.06	14.17
16 Sep 2005	0940	-15.92	-4.33	7.34	7.88	8.36
22 May 2003	2040	-22.20	-5.25	8.56	9.95	9.99
11 Jul 2003	0930	-14.84	0.11	11.65	11.85	12.74
Average		-17.98	-3.62	9.76	10.68	11.12

Table 14. MODIS brightness temperatures (C) over Vandenberg AFB for Category 3 radiosondes. Channels 27-32. are affected by water vapor absorption.

Date	UTC	Ch. 27	Ch. 28	Ch. 29	Ch. 31	Ch. 32
10 Jun 2003	1010	-24.93	-7.63	6.52	8.43	8.42
29 Jun 2003	1040	-27.63	-8.78	8.46	10.40	10.90
6 Jul 2003	0910	-30.60	-12.12	5.00	7.73	8.09
29 Apr 2004	0945	-16.69	-2.95	4.72	6.08	6.25
10 Jul 2004	1035	-27.71	-8.64	6.34	9.15	9.27
13 Jul 2004	0930	-19.82	-3.19	8.66	10.44	10.75
28 Jul 2004	1025	-22.84	-3.67	6.92	9.15	9.16
29 Jul 2004	0930	-17.76	-1.59	8.28	10.28	10.51
2 Aug 2004	1040	-26.30	-9.77	4.09	6.93	7.06
25 Aug 2005	1015	-17.57	-2.43	8.44	10.11	10.22
4 Sep 2005	0915	-25.87	-8.87	6.73	9.23	9.48
13 May 2006	1035	-32.62	-17.81	3.03	6.25	6.20
Average		-24.20	-7.29	6.43	8.68	8.86

V. CONCLUSION AND RECOMMENDATIONS

A. CONCLUSIONS

The Vandenberg AFB soundings and the data from buoy station 46011 provided a unique opportunity to test the parameterizations and analysis of the SEMEO program. This is the first time that the SEMEO program has been tested by both day and night cases within the littoral region. The current parameterizations within the SEMEO program were derived from day time only data that was collected both in and out of the littoral zone. One of the difficulties that had to be continually mitigated was the physical separation between the buoy and sounding launch site. Additionally, the satellite (MODIS) pass was not temporarily coincident with the radiosonde measurements. Screening processes were tailored around each test to alleviate these discrepancies.

There were 30 cases identified to test the cloud-top height algorithm within the SEMEO program. These 30 cases were tested using the reported SST and air temperature measured by buoy 46011. One of the SEMEO requirements within the algorithm to estimate cloud-top height is that the cloud-top brightness temperature be cooler than the surface temperature. Because of this physical requirement, three of the 30 cases using bouy-measured SST, and two of the 30 cases using bouy-measured air temperature for the surface values are not included in the overall statistics. The RMS error for the 27 cases using SST for the surface temperature is 160.0m, and 148.9m for the 28 cases using the buoy air temperature. Standard deviation is 226.6m (SST) and 206.6m (air temperature). The average cloud-top height is 532.4m (SST) and 556.0m (air temperature).

Additional comparisons were made within the 30 cases to isolate what was common among the cases that SEMEO represented well. There are 14 of the 27 SST cases that occurred at 1700 LT (day cases) and 13 that occurred at 0500LT (night cases). The RMS error for day cases is 154.3 meters and 165.9m for the night cases. The fractional error difference between the day and night cases were also calculated. For the day cases, the average cloud top height is 403.7 meters, yielding a fractional percentage error of 38%. For the night cases, the average cloud top height is 630.2 meters, yielding

a fractional error estimation of 26%. Another technique separated cases that had a temperature difference of greater than three degrees Celsius between Ch 4 and surface temperature. The RMS error for the 17 cases with greater than a three degree difference is 154m, and for the remaining 10 cases is 169.8m. The average cloud-top height estimate for the 17 cases is 637.9m, yielding a fractional percentage error of 24%. The average cloud-top height estimate for the remaining 10 cases is 412.7m with a fractional percentage error of 41%. Finally, a troughing feature aloft was evident in the 500mb heights chart for 11 of 15 cases listed in Table 8 that have an estimated height error of less than 100m. This troughing feature suppresses the subsidence allowing the boundary layer to deepen.

The refractive profile portion of the SEMEO program was tested with 14 cases. Five cases were from Category 1 (represented by approximately equal in magnitude temperature and dewpoint temperature differences within the targeted trapping region), and nine cases from Category 3 (represented by the magnitude of the dewpoint temperature difference within the targeted trapping layer being at least twice that of the temperature difference) For Category 1, the SEMEO predicted average trapping layer strength (ΔM) for the modified radiosondes with SST input is 41.3 with a resulting RMS error of 24.2 and a standard deviation of 7.0. For Category 1, four out of five cases were overestimated by the SEMEO program. The trapping layer depth for the SEMEO program is fixed at 100m. For the five Category 1 cases, the average trapping layer thickness measured by the modified radiosondes is 80.1 meters with a standard deviation of 28.3m. For Category 3, using SST as input, there are seven cases where the trapping layer strength is overestimated and two cases that are underestimated. The SEMEO predicted average strength for the modified radiosondes is 35.9. The corresponding RMS error is 5.8 with a standard deviation of 7.2. The average measured trapping layer thickness for the radiosondes is 66 meters with a standard deviation of 20m. The SEMEO program fixed 100m trapping layer overestimated eight out of nine Category 3 cases.

Nearly all Category 3 cases show a better comparison with measured ΔM than Category 1 cases. When analyzing the measured trapping layer strength generated by the

modified radiosondes, Category 1 is overestimated on average by $\sim 100\%$. The reason that SEMEO overestimates the strength for Category 1 may be related to the formula used to determine the strength (ΔM) that was created using linear regression techniques on a separate dataset. Within this formula, there is a parameter that is calculated, $\Delta T'$ that directly relates to the estimated trapping layer strength. The $\Delta T'$ average is $\sim 20\%$ higher for Category 1 cases than for Category 3. Additionally, the measured ΔM results from Category 3 are $\sim 33\%$ higher than Category 1, which highlights why the ΔM predicted results are more accurate for Category 3.

Overestimating the results of both trapping layer strength and thickness can give the user an inaccurate understanding of the refractive environment. Overestimations can result in predicting surface based ducts that are not present. Additionally if the duct thickness is overestimated, a user may erroneously believe that some frequencies will be trapped.

The final analysis focused on MODIS water vapor channels and images to see if there was a signature within the water vapor pattern that can be correlated with the moisture gradient profile within the trapping layer. The MODIS images from channels 20, 23, 27, 28, 29, 31, and 32 for 17 cases were analyzed and compared to their associated soundings. There were no definitive characteristics observed from the raw images or from image enhancements that could be correlated with the moisture gradient within the trapping layer. Image differencing techniques and enhancements of those images were also conducted with no definitive results.

B. RECOMMENDATIONS

The SEMEO algorithm used to determine cloud top height had varying degrees of success. The cases with deeper boundary layers, 500mb level troughing patterns, and greater than three degrees difference between satellite-measured cloud-top temperature and surface temperature produced the best results. These features could be accounted for through parameterizations within the algorithm to include assigning probabilities to give the user a better appreciation for the results. Additionally, the algorithm indicated more accurate results when air temperature measurements were used in the algorithm instead of

SST. Further analysis should be conducted to validate these findings and determine if parameterizations could account for these results.

The SEMEO algorithm used to determine the refractive trapping layer strength and depth was compared to 14 of the final 30 cases. The results were an overestimation of both, the trapping layer strength and thickness. Parameterizations within the algorithm could be made that would adjust the ΔM (linear) formula to account for varying boundary layer depths. Additionally the trapping layer should be able to adjust with varying boundary layers instead of being fixed at 100m for all cases.

In order to better understand the impact of upper level water vapor, additional transmittance and radiative transfer analysis should be incorporated into the study. This would allow the effect of water vapor concentrations above the inversion layer to be quantified. This, in conjunction with analyzing enhanced images, may allow a correlation to be realized between a water vapor features and humidity gradients within the trapping layer.

The final recommendation is to test the program with additional datasets to produce parameterizations that account for conditions that vary by region, seasons, and time of day.

LIST OF REFERENCES

American Meteorological Society, 2006: Glossary of Meteorology. [Available online at <http://amsglossary.allenpress.com/glossary/search?id=radio-horizon1>], last accessed August 2006.

CHAART, 2006: Sensor Specification GOES. [Available online at <http://geo.arc.nasa.gov/sgc/health/sensor/sensors/goes.html#spec>], last accessed August 2006.

Davidson, K. L., 2005: *Assessment of Atmospheric Factors in EM/EO Propagation*, MR4416 Course Notes, Department of Meteorology, Naval Postgraduate School, Monterey, CA, 263pp.

Goddard Space Flight Center, 2006: MODIS technical specifications. [Available online at <http://modis.gsfc.nasa.gov/about/specifications.php>], last accessed August 2006.

Kidder, S.Q., and Vonder Haar, T. H., 1995: *Satellite Meteorology: An Introduction*. Academic Press, San Diego. 466pp.

McBride, M. B., 2000: Estimation of Stratocumulus-topped boundary layer depth using sea surface and remotely sensed cloud-top temperatures. M.S. Thesis, Naval Postgraduate School, Monterey, CA, 101pp.

Ortenburger, L.N., Lawson, S.B., Patterson, B.J., 1985: *Radiosonde Data Analysis I*, Western Division GTE Government Systems Corporation, 1985.

Rogers, L.T., 1999: "Refractivity from clutter (RFC)," Presentation presented at the Naval Research Laboratory, Monterey, CA, 4 February 1999.

Rosenthal, J., Helvey, R., Battalino, T., Eddinton, L., Fisk, C., and Greiman, P., *Predicting the EM/EO Environment from Satellite, Synoptic and In-Situ Data Sources, Proceedings: Electromagnetic/Electro-Optics Prediction Requirements & Products Symposium.*, 1997.

San Francisco State University, 2006: [Available online at <http://virga.sfsu.edu/>], last accessed August 2006.

Sippican Inc., 2006: GPS Mark II micronsonde specifications. [Available online at <http://www.sippican.com/stuff/contentmgr/files/6f597c276e01b5e1f76a5fed153a0117/sh eet/gpsmark2.pdf>], last accessed August 2006.

THIS PAGE INTENTIONALLY LEFT BLANK

INITIAL DISTRIBUTION LIST

1. Defense Technical Information Center
Ft. Belvoir, Virginia
2. Dudley Knox Library
Naval Postgraduate School
Monterey, California
3. Professor Philip A. Durkee
Chairman, Department of Meteorology
Naval Postgraduate School
Monterey, California
4. Mary S. Jordan
Department of Meteorolgy
Naval Postgraduate School
Monterey, California
5. LCDR D. T. Derley
Department of Meteorolgy
Naval Postgraduate School
Monterey, California